

BEVTraj: Map-Free End-to-End Trajectory Prediction in Bird’s-Eye View with Deformable Attention and Sparse Goal Proposals

Minsang Kong, Myeongjun Kim, Sang Gu Kang, Hejiu Lu, Yupeng Zhong, Sang Hun Lee, *Member, IEEE*,

Abstract—In autonomous driving, trajectory prediction is essential for safe and efficient navigation. While recent methods often rely on high-definition (HD) maps to provide structured environmental priors, such maps are costly to maintain, geographically limited, and unreliable in dynamic or unmapped scenarios. Directly leveraging raw sensor data in Bird’s-Eye View (BEV) space offers greater flexibility, but BEV features are dense and unstructured, making agent-centric spatial reasoning challenging and computationally inefficient. To address this, we propose Bird’s-Eye View Trajectory Prediction (BEVTraj), a map-free framework that employs deformable attention to adaptively aggregate task-relevant context from sparse locations in dense BEV features. We further introduce a Sparse Goal Candidate Proposal (SGCP) module that predicts a small set of realistic goals, enabling fully end-to-end multimodal forecasting without heuristic post-processing. Extensive experiments show that BEVTraj achieves performance comparable to state-of-the-art HD map-based methods while providing greater robustness and flexibility without relying on pre-built maps. The source code is available at <https://github.com/Kongminsang/bevtraj>.

Index Terms—Trajectory prediction, autonomous vehicles, deep learning, sensor fusion, deformable attention, bird’s-eye-view.

I. INTRODUCTION

TRAJECTORY prediction plays a pivotal role in autonomous driving, enabling vehicles to anticipate the future movements of surrounding agents and make safer, more informed decisions. Beyond individual agent-level forecasting, trajectory prediction also has broader implications for intelligent transportation systems, supporting traffic safety assessment, flow analysis, and risk identification. Recent transportation studies highlight that high-resolution trajectory data and structured scene reconstruction are essential for understanding traffic dynamics and reliably extracting motion patterns from large-scale observations [1]–[3], underscoring its role in improving overall traffic efficiency and safety.

Manuscript received July 10, 2025

Minsang Kong and Myeongjun Kim are with the Department of Automobile and IT Convergence, Kookmin University, 77 Jeongneung-ro, Seongbuk-gu, Seoul 02707, Republic of Korea (e-mail: gms0725@kookmin.ac.kr; thd3266772@kookmin.ac.kr).

Sang Gu Kang is with the Department of Automotive Engineering, Kookmin University, 77 Jeongneung-ro, Seongbuk-gu, Seoul 02707, Republic of Korea (e-mail: k84652001@kookmin.ac.kr).

Hejiu Lu and Yupeng Zhong are with the Graduate School of Automobile and Mobility, Kookmin University, 77 Jeongneung-ro, Seongbuk-gu, Seoul 02707, Republic of Korea (e-mail: lhj17@kookmin.ac.kr; zzzsignal@kookmin.ac.kr).

Sang Hun Lee is with the Graduate School of Automobile and Mobility, Kookmin University, 77 Jeongneung-ro, Seongbuk-gu, Seoul 02707, Republic of Korea (e-mail: shlee@kookmin.ac.kr, ORCID: <https://orcid.org/0000-0001-8888-2201>).

Minsang Kong and Myeongjun Kim have contributed equally.

The corresponding author is Sang Hun Lee (e-mail: shlee@kookmin.ac.kr).

Despite these advantages, trajectory prediction remains inherently challenging due to the multimodal nature of agent behaviors and complex agent–environment interactions. Accurate forecasting requires modeling structural constraints such as road topology and scene geometry, for which map information is commonly employed. While standard-definition (SD) maps provide broad but coarse static context, high-definition (HD) maps offer detailed layouts and semantics that better support fine-grained motion reasoning. However, HD maps are costly to construct and maintain, geographically limited, and difficult to update in real time, restricting map-dependent methods to pre-mapped regions and reducing their adaptability to dynamic changes such as construction zones or accidents.

For these reasons, recent works construct local HD maps online from raw sensors, enabling autonomous vehicles to operate in unmapped areas and adapt to dynamic road conditions [4]–[6]. However, relying solely on reconstructed maps remains problematic: HD maps are inherently unavailable or unreliable in irregular or rapidly changing environments, and online map construction is still susceptible to perception errors such as misclassification, missing elements, positional inaccuracies, and limited predefined semantics. Consequently, to fully exploit the rich geometric and semantic cues that are not captured by map representations alone and to minimize information loss, trajectory prediction must directly leverage raw sensor data. Fig. 1 contrasts this direct sensor-based paradigm with the conventional map-based approaches.

Despite its importance, directly leveraging raw sensor data introduces new challenges. Unlike vectorized HD maps that provide sparse, semantically structured, and topology-aware representations, sensor-derived Bird’s-Eye View (BEV) features are inherently dense, image-like, and unstructured, requiring the model to jointly reason about both what each feature represents and where it is located, thereby making spatial reasoning substantially more complex. This difficulty is further amplified by the intrinsic nature of trajectory prediction: while perception tasks benefit from globally dense and largely object-agnostic representations, trajectory prediction is fundamentally agent-centric and conditional, where the spatial context relevant to future motion depends on the target agent’s state, behavior mode, and prediction horizon. Consequently, only a small and dynamically varying subset of the scene is informative at each stage, a property that cannot be effectively captured by global attention [7], fixed local-window mechanisms [8], or convolutional aggregation. Naively processing the entire BEV grid is thus both computationally inefficient and prone to diluting critical cues with irrelevant information.

These observations suggest that the central challenge of BEV-based, map-free trajectory prediction is not merely how

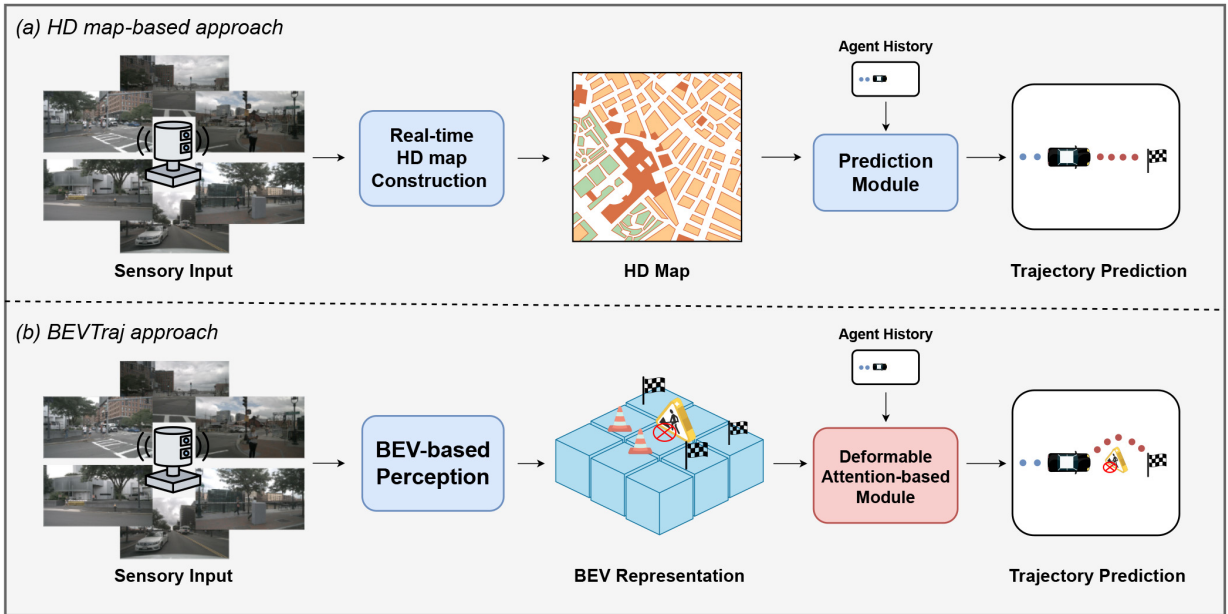


Fig. 1. Two possible approaches for trajectory prediction in the absence of a pre-defined HD map. The first approach (top) constructs an HD map in real time and applies conventional HD map-based prediction methods. The second approach (bottom), proposed in this study as BEVTraj, directly predicts trajectories by leveraging BEV features extracted from raw sensor data.

to encode dense BEV features, but how to selectively and adaptively aggregate task-relevant spatial context in a computationally efficient and agent-specific manner. To address this issue, we propose **Bird’s-Eye View Trajectory Prediction (BEVTraj)**, a framework that performs trajectory prediction through adaptive, agent-centric context aggregation grounded in deformable attention [9]. Specifically, BEVTraj first constructs BEV representations directly from raw sensor data and then selectively gathers context for each agent from a sparse set of dynamically predicted sampling locations instead of exhaustively attending to the entire BEV grid, enabling efficient, geometry-aware, and agent-centric information extraction from dense BEV representations.

In addition, we introduce a *Sparse Goal Candidate Proposal (SGCP)* module to address a fundamental limitation of existing goal-based approaches, which rely on densely sampled or pre-defined anchors that are inflexible and often produce redundant or physically implausible candidates. Rather than enumerating dense goals, SGCP directly predicts a small set of sample-adaptive and realistic proposals conditioned on the scene context, enabling efficient and reliable multimodal forecasting with minimal candidates and eliminating the need for heuristic post-processing such as non-maximum suppression (NMS).

II. RELATED WORK

A. Trajectory Prediction with HD Maps

HD-map-based trajectory prediction exploits lane geometry, road topology, and traffic semantics as strong priors to constrain plausible futures. Early methods often rasterize HD maps into BEV images and encode them with CNNs [10]–[14]. While rasterization simplifies feature extraction, it can blur lane directionality and break topological continuity, which weakens fine-grained agent–map interaction modeling. To

preserve structure, vectorized representations explicitly encode lanes as polylines/graphs with connectivity. Representative works such as VectorNet [15] and LaneGCN [16] model agent–lane and lane–lane relations via hierarchical encoding and graph propagation, and LaneATT [17] further strengthens lane-centric semantic extraction for interaction reasoning.

Beyond map encoding, handling the intrinsic multi-modality of future motion is another key challenge. Goal-conditioned pipelines such as TNT [18] decouple high-level intention (endpoint) from low-level trajectory refinement, and dense goal sampling variants (e.g., DenseTNT) improve coverage of diverse behaviors [18]. More recently, transformer-based architectures become dominant by unifying heterogeneous scene inputs and capturing long-range dependencies, including Wayformer [19], DeMo [20], and query-based decoders such as MTR [21] and SceneTransformer [22]. Extensions like QCNet [23] emphasize query-centric goal reasoning, while FIM [24] incorporates reward-guided inference to inject planning priors. Despite strong accuracy, these paradigms fundamentally rely on the availability and correctness of HD maps; missing lane segments, outdated topology, and domain shifts in map quality can severely degrade prediction and hinder scalability, motivating map-free forecasting.

B. Map-Free Trajectory Prediction

To reduce the cost and brittleness introduced by HD maps, recent studies explore map-free trajectory prediction [25]–[28], where future motion is inferred from observed dynamics and interactions without explicit lane topology. A common line of work treats the problem as generative modeling in trajectory space. For example, DLow [29] learns a latent flow to generate diverse futures and is widely used as a strong map-free baseline. Transformer-based sequence models such

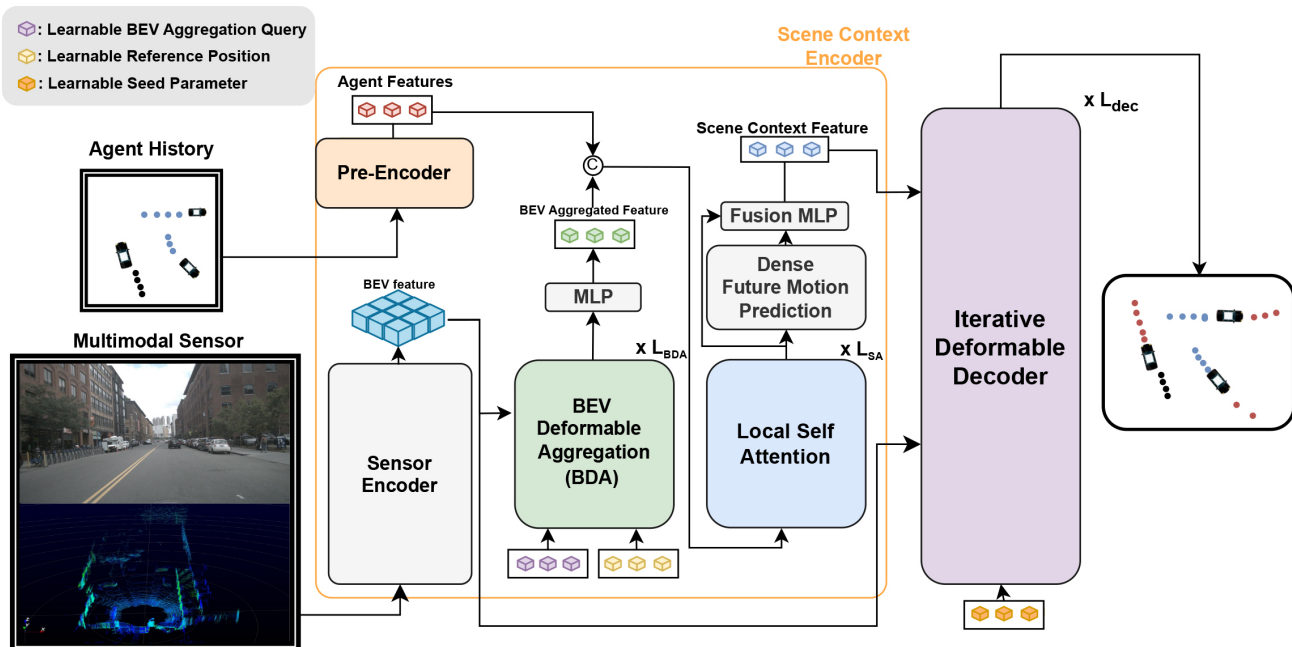


Fig. 2. Overall architecture of BEVTraj. Sensor Encoder processes multimodal sensor data (e.g., camera images, LiDAR point clouds) to generate BEV feature, while Pre-Encoder captures agent motion history. BEV Deformable Aggregation (BDA) module efficiently compresses BEV feature into a compact representation, which is then integrated with Pre-Encoder’s output through local self-attention. Iterative Deformable Decoder predicts the target agent’s trajectory and iteratively refines it using both BEV feature and scene context feature.

as AgentFormer [30] further enhance temporal and inter-agent reasoning within a unified attention framework, improving multi-modal prediction without map priors.

Another effective direction is graph-based interaction modeling, which explicitly represents agents as relational graphs. CRAT-Pred [25] leverages a crystal-graph representation with multi-head attention to strengthen spatial interaction modeling, while GATraj [31] integrates graph neural networks and attention to enrich relational reasoning and achieves competitive performance on nuScenes. Multi-level spatio-temporal designs such as ML-STM [26] reinforce interactions across different temporal scales to better handle complex dynamics. However, many map-free approaches still operate primarily in trajectory/interaction space, where scene geometry and spatial constraints are only implicitly captured. This can be insufficient in topologically complex situations (e.g., merges/splits) or occlusion-heavy scenes, where structured spatial priors are crucial to rule out physically implausible futures.

C. Map-Free Trajectory Forecasting via BEV Representation

BEV representation provides a geometry-consistent plane for aggregating spatial, temporal, and semantic cues, enabling unified reasoning over scene layout, motion, and interactions. Recent BEV perception frameworks demonstrate scalable feature lifting and projection into BEV [32]–[34]. A key driver behind modern BEV transformers is deformable attention [9], which performs sparse sampling to focus computation on geometrically relevant regions while retaining relational modeling capacity. This mechanism underpins architectures such as BEVFormer [35], BEVFormerV2 [36], and Ego3RT [37],

enabling effective cross-view fusion and temporal reasoning in dynamic scenes.

Beyond camera-centric pipelines, radar–camera BEV perception has gained attention due to radar’s robustness under adverse weather and long-range sensing capability. Representative frameworks such as RCBEVDet [38] and RCBEVDet++ [39] show that radar reflections can be lifted into BEV and fused with camera features to improve spatial completeness and dynamic cue extraction, suggesting BEV representations naturally extend to multimodal settings.

For forecasting, early BEV predictors constructed rasterized BEV maps from HD-map geometry and processed them with CNNs/MLPs [40]–[42], which still inherit HD-map dependency. In contrast, vision-centric frameworks such as FIERY [43], BEVerse [44], and TBP-Former [45] learn BEV dynamics directly from sensors without maps, confirming that BEV can serve as a structured spatial prior for map-free forecasting. Nevertheless, many existing BEV forecasting pipelines remain vision-centric or weakly multimodal, which may limit robustness under adverse sensing conditions. Motivated by this gap, BEVTraj extends deformable-attention BEV modeling toward a fully sensor-based, map-free formulation: it constructs BEV features directly from raw multi-sensor data and jointly models temporal dependencies and inter-agent interactions within a unified geometry-aware representation, enabling robust end-to-end trajectory forecasting under map-free conditions.

III. METHOD

In this section, we present BEVTraj, a framework that predicts the multimodal future distribution of the target agent’s trajectory. BEVTraj comprises two main modules: *Scene Context Encoder*, and *Iterative Deformable Decoder*. The Scene

Context Encoder generates *scene-level context features* by capturing complex interactions within the scene, utilizing the historical states of agents and the BEV features extracted from raw sensor data. Subsequently, the Iterative Deformable Decoder sequentially predicts multiple goal candidates and their corresponding initial trajectories for the target agent, and refines these predictions iteratively. An overview of BEVTraj is shown in Fig. 2.

A. Scene Context Encoder

A clear understanding of complex interactions within the scene context is crucial for trajectory prediction. Motion Transformer (MTR) [46] encodes scene context by utilizing a PointNet-like [47] polyline encoder to vectorize road maps and agent trajectories, applying local self-attention to preserve spatial locality and enhance memory efficiency, and using an auxiliary regression head to predict dense future trajectories of surrounding agents to improve interaction modeling, which provides an explicit supervision signal for agent-to-agent interaction modeling at the scene (system) level. The Scene Context Encoder builds upon this design and introduces three sub-modules: *Sensor Encoder*, *Pre-Encoder*, and *BEV Deformable Aggregation (BDA)* modules.

1) *Sensor Encoder*: As in object detection, both semantic and geometric information are essential for trajectory prediction, motivating BEVTraj to adopt a sensor fusion architecture that integrates images and point clouds. This raises a critical question: which spatial domain is best suited for representing essential features? BEVTraj adopts the BEV space for the following reasons. First, since trajectory prediction is conducted in BEV space, this alignment ensures consistency between the prediction output and the feature representation. Moreover, Liu et al. [48] argued that lidar point clouds and camera images are fundamentally different modalities and that fusing them in BEV space is the most appropriate approach. Based on these insights, BEVTraj employs BEVFusion [48]—an off-the-shelf sensor fusion architecture—as the Sensor Encoder to generate a BEV feature map $\mathbf{B} \in \mathbb{R}^{C \times H \times D}$, where H and W denote the spatial dimensions. Since BEVTraj follows the BEV paradigm [48]–[50], it can be seamlessly integrated into modern BEV-based autonomous driving systems. Meanwhile, the BEVFusion module serves as an off-the-shelf sensor encoder and can be readily replaced with any alternative BEV-based fusion architecture.

2) *Pre-Encoder*: Previous studies categorize scene interaction encoding into two approaches: preserving or compressing the temporal dimension. The former allows for temporal positional encoding and better captures motion tendencies. In contrast, the latter compresses the temporal axis, improving parameter efficiency by increasing representational capacity with the same number of parameters. MTR adopts the latter approach, which limits its ability to model motion dynamics. To address this limitation, the Scene Context Encoder incorporates a Pre-Encoder that applies temporal self-attention (as introduced by Girgis et al. [51]) prior to temporal dimension. enables more effective modeling of motion tendencies before local self-attention is applied. Furthermore, social self-attention

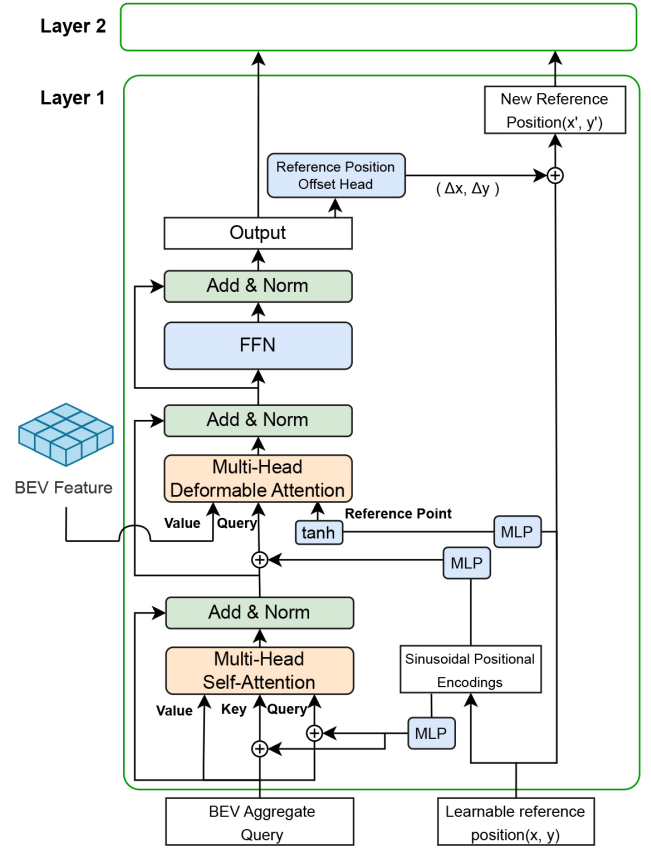


Fig. 3. Architecture of the BEV Deformable Aggregation (BDA) module. The BA queries and learnable reference positions are iteratively refined through self-attention and deformable cross-attention layers. The final BA queries are passed through an MLP to produce BEV aggregated features.

(also introduced by Girgis et al. [51]) follows temporal self-attention to capture inter-agent interactions at each timestep. Finally, a PointNet-like encoder transforms the representation from $\mathbb{R}^{N_a \times t \times d}$ into an *agent feature* $\mathbf{A} \in \mathbb{R}^{N_a \times D}$, where N_a denotes the number of agents in the scene and t represents the number of past temporal steps.

3) *BEV Deformable Aggregation*: As described in Section I, sensor-derived Bird’s-Eye View (BEV) features are inherently dense, image-like, and unstructured. BEVTraj encodes road topology and physical constraints directly from raw sensor data into a BEV feature map \mathbf{B} , which makes global attention—computing attention scores across the entire BEV grid—computationally prohibitive. To address this challenge, we propose the *BEV Deformable Aggregation (BDA)* module, which selectively attends to a compact set of key spatial locations in \mathbf{B} and aggregates them into a fixed number of vectors, referred to as the *BEV aggregated feature* $\in \mathbb{R}^{N_m \times D}$. Here, N_m denotes the number of selected spatial locations used for aggregation, enabling computationally efficient attention operations.

The structure of BDA is inspired by DAB-Deformable-DETR [9], [52], as illustrated in Fig. 3. BDA is structured around a BEV Aggregate (BA) queries, initialized as zero, and learnable reference positions, which are randomly initialized and processed with sinusoidal positional encoding followed

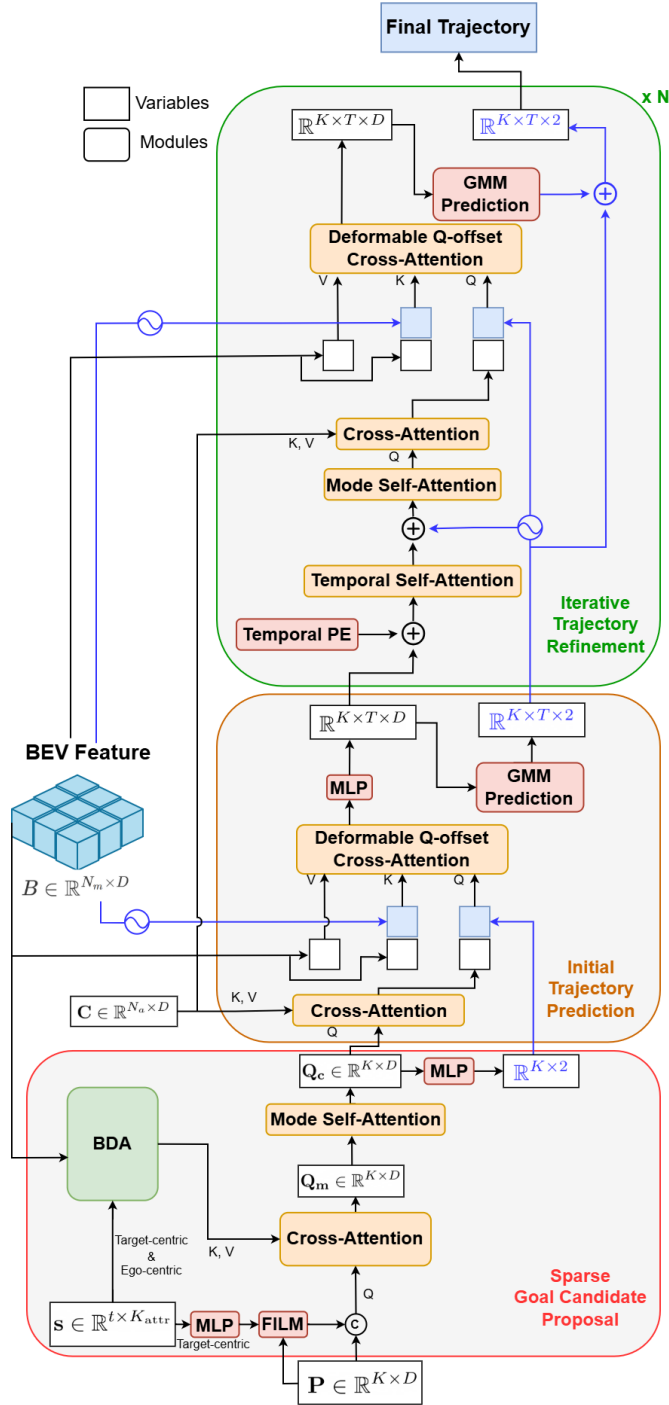


Fig. 4. Structure of the Iterative Deformable Decoder, consisting of three sub-modules for multimodal trajectory prediction: goal proposal, initial prediction, and iterative refinement. Deformable attention is used in each stage to process BEV features.

by a multi-layer perceptron (MLP) to obtain positional embeddings. These embeddings are added element-wise to the BA queries and passed through a self-attention layer. In the deformable cross-attention step, the BA queries interact with the BEV feature map B , leveraging the learnable reference positions as anchor points to adaptively aggregate spatial information. A lightweight MLP head then computes offsets, which are used to update the reference positions. This process is

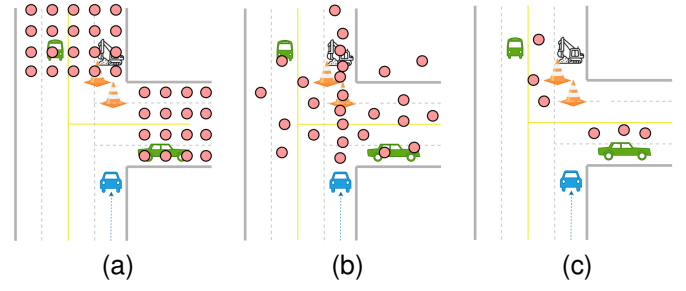


Fig. 5. Comparison of goal candidate proposal methods. (a) DenseTNT generates dense goal candidates along lanes. (b) MTR defines intention points via k-means clustering. (c) Our SGCP module predicts a sparse set of goal candidates conditioned on the agent's dynamic state and the BEV feature map.

repeated across multiple layers, progressively refining both the BA queries and their associated reference positions. Finally, the refined BA queries are passed through a final MLP to produce BEV aggregated feature.

By adopting this *position-based iterative refinement* structure, BDA offers the following advantages: (1) It allows reference points to continuously refine their spatial locations based on aggregated BEV information, ensuring that each BA query attends to a specific spatial region while dynamically adapting its position to the underlying data distribution. (2) This adaptability further facilitates the integration of local self-attention, as introduced in MTR, by providing explicit spatial anchors for each scene element. Notably, the normalized reference points are transformed into the target agent's coordinate frame, accounting for both the ego vehicle's state (position and orientation) and the predefined coverage area of B .

The BEV aggregated feature produced by BDA is then concatenated with the agent feature A generated by Pre-Encoder, followed by local self-attention to model interactions between surrounding agents and the environment. Subsequently, dense future motion prediction is performed for each agent to account for agent interactions over the future horizon, resulting in the construction of the *scene context feature* $C \in \mathbb{R}^{N_a \times D}$.

B. Iterative Deformable Decoder

The *Iterative Deformable Decoder* predicts and refines the multimodal future trajectory of the target agent based on B and C , as illustrated in Fig. 4. It comprises three sub-modules: *Sparse Goal Candidate Proposal*, *Initial Trajectory Prediction*, and *Iterative Trajectory Refinement*. Each module employs deformable attention [9] to selectively and adaptively aggregate agent-centric context from the dense BEV representation. For simplicity, residual connections, normalization layers, feedforward networks, and some MLP components within the decoder are omitted in the following descriptions.

1) *Sparse Goal Candidate Proposal*: As illustrated in Fig. 5, many existing trajectory prediction methods rely on generating a dense set of goal candidates, followed by trajectory exploration conditioned on these candidates. DenseTNT [53] samples goals densely along lanes, while Motion Transformer (MTR) [46] predefines intention points via k-means clustering on training data. Although such dense

or anchor-based designs can alleviate mode collapse through brute-force diversity, they are inherently inflexible: most goal candidates are predefined and fail to adapt to scene-specific structures or the dynamic state of the target agent, and may even fall outside physically plausible or navigable regions. To overcome this limitation, we propose the *Sparse Goal Candidate Proposal (SGCP)* module, which directly predicts a small set of sample-adaptive, realistic, and reliable goal candidates. By explicitly conditioning goal generation on both the target agent’s dynamic state \mathbf{s} and the BEV feature map \mathbf{B} , SGCP maintains strong prediction performance with only a limited number of sparse goals.

We next describe the architectural design and operational pipeline of SGCP in detail. SGCP adopts learnable seed parameters $\mathbf{P} \in \mathbb{R}^{K \times D}$ to represent K latent behavior modes, where each seed functions as a mode query responsible for proposing one goal hypothesis. Unlike anchor-based approaches that rely on predefined spatial priors, these queries are learned end-to-end and must themselves maintain sufficient diversity. To incorporate the target agent’s motion history as an informative positional prior and to prevent different queries from collapsing into similar representations, the dynamic state $\mathbf{s} \in \mathbb{R}^{t \times K_{attr}}$ is first encoded by an MLP and injected into the mode queries through Feature-wise Linear Modulation (FiLM) [54]. Concretely, FiLM predicts query-specific scaling and shifting parameters conditioned on the history embedding and applies an affine transformation to each query independently. This lightweight conditioning modulates each query separately, enabling distinct, mode-dependent representations and explicitly mitigating mode collapse during early-stage goal generation.

To further incorporate scene context into the goal queries, we employ the BEV Deformable Aggregation (BDA) module, which is also used in the Scene Context Encoder, to selectively aggregate BEV features relevant to the target agent’s goal prediction. Specifically, decoder-side BDA aggregates features using target-aware reference points generated from the target agent’s motion history, collecting scene information from spatial regions most likely to influence the predicted goals. BDA also addresses a fundamental spatial misalignment issue: BEV features are defined in the ego-centric coordinate frame, whereas trajectories are predicted in the target-agent-centric frame. To resolve this discrepancy, the spatial coordinates of the aggregated BEV tokens are explicitly transformed into the target-agent-centric frame and used as positional keys for the subsequent cross-attention, producing mode-specific features $\mathbf{Q}_m \in \mathbb{R}^{K \times D}$.

The resulting mode features are further refined by a mode self-attention layer that models interactions and competition among the K modes, yielding content queries $\mathbf{Q}_c \in \mathbb{R}^{K \times D}$. Placing this self-attention after the BEV cross-attention ensures that \mathbf{Q}_m already encodes rich scene context, enabling meaningful information exchange across modes and promoting distinct spatial roles for each query. A lightweight MLP head then directly regresses \mathbf{K} goal coordinates $\in \mathbb{R}^{K \times 2}$ in the target-centric space, generating a sparse set of realistic and behaviorally distinct goal candidates.

Beyond the above operational pipeline, we further highlight

several architectural design choices that make SGCP efficient and robust, among which a key factor is the explicit decomposition of goal reasoning into two sequential stages. Decoder-side BDA first performs target-aware aggregation over the BEV feature map using a relatively large number of reference tokens (e.g., 256), forming a dense pool of goal-relevant scene features and providing broad spatial coverage (spatial exploration). A subsequent cross-attention then employs only a small set of mode queries to selectively attend to these aggregated tokens and refine them into sparse goal hypotheses (goal selection). This separation enables sufficient exploration while keeping the number of prediction modes compact. In contrast, methods such as MTR rely solely on mode queries for both exploration and selection, causing spatial coverage to scale with the number of modes and thus requiring many queries to capture diverse futures. By delegating dense exploration to BDA and reserving the queries for structured selection, SGCP achieves stable optimization and behaviorally diverse predictions with only a small set of realistic goal candidates.

In addition, the decoder-side BDA predicts reference points by encoding the target agent’s past trajectory under both target-centric and ego-centric coordinate systems to provide complementary motion cues for BEV aggregation. The target-centric representation offers normalized relative dynamics, while the ego-centric one maintains direct alignment with the BEV feature space. Combining both yields more reliable spatial anchoring and more effective feature aggregation.

2) *Initial Trajectory Prediction*: The *Initial Trajectory Prediction (ITP)* module is designed to generate initial trajectories from the proposed goal candidates. ITP operates as follows: First, it performs cross-attention between the content queries \mathbf{Q}_c and the scene context feature \mathbf{C} , incorporating interactions with surrounding agents. It then applies deformable cross-attention over the BEV feature map \mathbf{B} , where the goal predictions from SGCP serve as reference points and offsets are computed from \mathbf{Q}_c . By using the predicted goals as reference points, each mode can attend to road structures near its predicted destination, reducing unnecessary computation.

Following prior work [46], [52], [55], sinusoidal positional encoding is applied to the predicted goal positions, which are used as positional queries. The resulting features are passed through an MLP to expand the channel dimension to $T \times D$, and then reshaped into $\mathbb{R}^{K \times T \times D}$ introducing a temporal dimension that is maintained in subsequent modules. This temporal bottleneck strategy naturally aligns with the functional requirements of each module: the goal candidate proposal does not require temporal reasoning, whereas trajectory prediction and refinement inherently do.

Finally, the resulting embeddings are used to predict the multimodal distribution of initial trajectories via a Gaussian Mixture Model (GMM) at each time step.

3) *Iterative Trajectory Refinement*: Following the paradigm commonly adopted in detection models—where each decoder block refines the output of the previous one and uses explicit position encodings as positional queries [9], [52], [55], [56], MTR [46] extended this framework to trajectory prediction. Similarly, the *Iterative Trajectory Refinement (ITR)* module in BEVTraj adopts this paradigm to iteratively refine the initial

trajectories predicted by ITP.

The ITR module operates as follows: it first applies temporal self-attention and mode self-attention to the decoder embedding output from ITP, denoted as $\in \mathbb{R}^{K \times T \times D}$. It then performs cross-attention and deformable cross-attention with the scene context feature \mathbf{C} , where offsets are derived from the query embeddings, as in ITP. Finally, refinement offsets $(\Delta x, \Delta y)$ are computed to update the trajectory predictions from the previous refinement block.

While the ITR module is structurally similar to the MTR decoder, its key distinction lies in distributing queries across future timestamps. This allows temporal self-attention to treat vectors at each time step as independent tokens, enabling better modeling of motion tendencies. Moreover, because the target agent’s position at each time step is used as a reference point for deformable attention, the module can selectively retrieve time-specific contextual features from the BEV feature map \mathbf{B} .

C. Losses

The overall training objective is defined as the sum of four loss components:

$$\mathcal{L} = \lambda_{\text{goal}}\mathcal{L}_{\text{goal}} + \lambda_{\text{disp}}\mathcal{L}_{\text{disp}} + \lambda_{\text{dense}}\mathcal{L}_{\text{dense}} + \lambda_{\text{multi}}\mathcal{L}_{\text{multi}} \quad (1)$$

Each term in Eq. (1) corresponds to a specific prediction module and is described in detail below.

1) *Goal Loss* ($\mathcal{L}_{\text{goal}}$): We generate K goal candidates $\{\hat{g}_k\}$ and supervise the one closest to the ground-truth final position g using an ℓ_2 regression loss:

$$\mathcal{L}_{\text{goal}} = \min_k \|\hat{g}_k - g\|_2^2 \quad (2)$$

2) *Displacement Loss* ($\mathcal{L}_{\text{disp}}$): Following Ye et al. [57], each goal candidate predicts its own final displacement error (FDE) as a scalar. These predictions are trained using a Smooth ℓ_1 loss:

$$\mathcal{L}_{\text{disp}} = \frac{1}{K} \sum_{k=1}^K \text{SmoothL1}(\hat{d}_k, \|\hat{g}_k - g\|_2) \quad (3)$$

3) *Dense Trajectory Loss* ($\mathcal{L}_{\text{dense}}$): To supervise dense future trajectory regression, we apply an ℓ_1 loss as proposed by Shi et al. [46]:

$$\mathcal{L}_{\text{dense}} = \|\hat{Y} - Y\|_1 \quad (4)$$

where \hat{Y} and Y denote the predicted and ground-truth future trajectories, respectively.

4) *Multimodal Loss* ($\mathcal{L}_{\text{multi}}$): For multimodal trajectory prediction, we follow Girgis et al. [51] and adopt the combined loss $\mathcal{L}_{\text{multi}}$, which integrates four components:

$$\mathcal{L}_{\text{multi}} = \lambda_{\text{nl}}\mathcal{L}_{\text{nl}} + \lambda_{\text{kl}}\mathcal{L}_{\text{kl}} + \lambda_{\text{ent}}\mathcal{L}_{\text{ent}} + \lambda_{\text{aux}}\mathcal{L}_{\text{aux}} \quad (5)$$

These four components are computed at each decoder layer and averaged to form the final $\mathcal{L}_{\text{multi}}$. Each component is defined as follows:

- *Negative Log-Likelihood Loss* (\mathcal{L}_{nl}): Measures the likelihood of the ground-truth trajectory under the predicted

mode distributions, weighted by their posterior probabilities.

- *KL Divergence Loss* (\mathcal{L}_{kl}): Encourages alignment between the predicted prior and posterior distributions over trajectory modes.
- *Entropy Regularization* (\mathcal{L}_{ent}): Promotes mode sharpness by penalizing high-entropy trajectory distributions within each mode.
- *Auxiliary Displacement Loss* (\mathcal{L}_{aux}): Penalizes the displacement error of the best-matching predicted mode with respect to the ground-truth.

All loss weights are fixed across experiments. Specifically, we set $\lambda_{\text{goal}} = 15$, $\lambda_{\text{disp}} = 5$, $\lambda_{\text{dense}} = 1$, $\lambda_{\text{multi}} = 1$, $\lambda_{\text{nl}} = 1$, $\lambda_{\text{ent}} = 10$, $\lambda_{\text{KL}} = 10$, and $\lambda_{\text{aux}} = 100$.

IV. EXPERIMENTS

A. Datasets

1) *nuScenes*: We evaluate BEVTraj on *nuScenes dataset* [58], a large-scale autonomous driving dataset collected in Boston, USA, and Singapore. It encompasses diverse driving environments, including intersections, urban streets, residential areas, and industrial zones. In this study, we focus on the trajectory prediction task, which is defined as predicting the future 6 seconds of agent motion given 2 seconds of past trajectory as input. We use the official prediction split of the dataset, consisting of approximately 32k training samples and 9k validation samples.

2) *Argoverse 2 Sensor dataset*: We also utilize the Argoverse 2 Sensor dataset [59], a large-scale autonomous driving dataset collected across six U.S. cities, including Miami, Pittsburgh, and Washington, D.C. It comprises 1,000 vehicle logs, each approximately 15 seconds long, totaling 4.2 hours of driving data. Each log contains synchronized sensor data from two 32-beam lidars and nine cameras (seven ring cameras and two stereo cameras), captured at 10 Hz and 20 Hz, respectively.

Unlike nuScenes, which provides predefined target agents, Argoverse 2 Sensor does not specify prediction targets. Therefore, we extract 35k training samples and 7k validation samples by identifying suitable target agents based on object type, motion, trajectory validity, and proximity to the ego-vehicle. Each sample consists of 2 seconds of past and 6 seconds of future trajectory, sampled at 10 Hz. This setting is aligned with the nuScenes-based setup to ensure fair comparison.

B. Implementation and Training

1) *Implementation Details*: For data preprocessing, agent history was normalized to the target agent’s coordinate system for both datasets, following Feng et al. [60]. Additionally, for nuScenes, we interpolate the agent history from 2Hz to 10Hz to match the sampling frequency of Argoverse. To improve generalization, basic data augmentation techniques—rotation, scaling, flipping, and cropping—are applied exclusively to image inputs; no augmentation is applied to point clouds or agent trajectories. To mitigate occlusion issues, multi-sweep point clouds are aggregated and warped based on the ego vehicle’s motion before being input into the model.

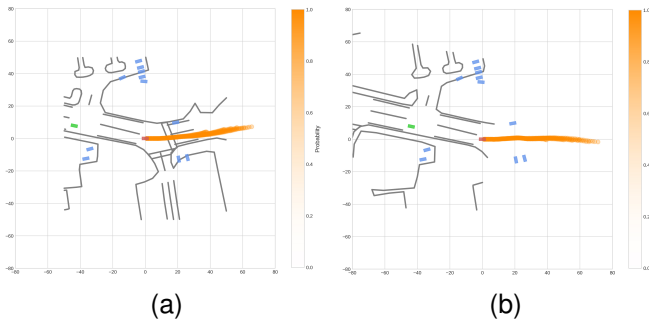


Fig. 6. Comparison of HD map ranges used in HD map-based models. Red indicates the target agent, and green indicates the ego vehicle. (a) The 50-meter map is aligned with the target agent at the center. (b) The 50-meter map is aligned with the ego vehicle at the center. In the absence of a pre-built HD map, real-time HD map construction from raw sensor data typically results in maps centered on the ego vehicle.

The overall BEVTraj architecture follows an encoder-decoder structure. Each sub-module in the Scene Context Encoder is designed as follows: the Pre-Encoder employs a temporal-social attention mechanism with two stacked layers, while the BDA module uses 256 BEV aggregate queries and applies deformable aggregation through three stacked layers. The local self-attention component consists of six layers in total. The entire architecture uses a channel dimension of 256 for each token representation (*e.g., content queries, positional queries*) across all attention modules.

2) *Training Details*: Prior to training for the trajectory prediction task, we pre-train the Sensor Encoder on a BEV map segmentation task to enhance its ability to capture static scene elements. The model is implemented in PyTorch and optimized using AdamW with a weight decay of 0.01. We adopt a warm-up cosine learning rate schedule, linearly increasing the learning rate from 0 to 1.0×10^{-4} over the first 3 epochs and subsequently decaying it to 5.0×10^{-6} following a cosine annealing strategy for the remainder of training. Dropout and layer normalization are applied to decrease overfitting. We train the model for 15 epochs with a batch size of 8 using four NVIDIA RTX 4090 GPUs. In order to jointly optimize different aspects of trajectory prediction, our model is trained end-to-end using multiple loss functions shown in Eq. (1) and loss weights summarized in Section II.C.

C. Quantitative Results

1) *Comparison with HD Map-Based Methods*: To the best of our knowledge, this study is the first to perform trajectory prediction using only raw sensor data without pre-built HD maps. Sensor-based perception is inherently limited to local, ego-centric observations, typically within 50 m in BEV-based pipelines such as BEVFusion [48] and BEVerse [61]. As illustrated in Fig. 6, real-time maps constructed from raw sensor data are naturally centered on the ego vehicle. Therefore, for a fair comparison, we restrict the HD map input of the map-based baseline methods to a ± 50 m range centered at the ego vehicle when conducting our evaluation. Following the official nuScenes prediction benchmark, we report standard

TABLE I
PERFORMANCE COMPARISON OF TRAJECTORY PREDICTION ON THE VALIDATION SET OF *nuScenes* DATASET.

Method	minADE ₅ ↓	minADE ₁₀ ↓	minFDE ₁ ↓	minFDE ₁₀ ↓	Miss Rate ↓
Autobot	1.9566	1.1649	8.8171	2.3294	0.3229
MTR	1.2926	1.0446	7.2689	2.2840	0.4240
Wayformer	1.4034	0.9877	7.9707	2.2483	0.3868
DeMo	1.3137	1.0424	7.1679	2.1806	0.3399
BEVTraj (Ours)	1.3953	0.9051	8.1975	1.8964	0.2783

TABLE II
PERFORMANCE COMPARISON OF TRAJECTORY PREDICTION ON THE VALIDATION SET OF *Argoverse 2 Sensor* DATASET.

Method	minADE ₅ ↓	minADE ₁₀ ↓	minFDE ₁ ↓	minFDE ₁₀ ↓	Miss Rate ↓
Autobot	1.3284	0.7430	6.9975	1.6861	0.2136
MTR	0.9243	0.7944	5.8264	1.9926	0.3361
Wayformer	1.0454	0.6721	6.2511	1.6775	0.2181
DeMo	0.8528	0.6426	5.2801	1.4964	0.1976
BEVTraj (Ours)	1.0412	0.6525	6.6665	1.6434	0.2144

TABLE III
THE RESULTS OF OCCUPANCY PREDICTION EVALUATED OVER A 100×100 M RANGE.

Method	IoU ↑
FIERY [62]	36.7
StretchBEV [63]	37.1
ST-P3 [64]	38.9
BEVerse [61]	40.9
PowerBEV [65]	39.3
UniAD [66]	40.2
FusionAD [67]	51.5
BEVTraj (GT-hist)	78.2
BEVTraj (E2E)	52.7

multimodal forecasting metrics including minADE, minFDE, and Miss Rate.

Tables I and II show that BEVTraj achieves competitive performance against HD map-based methods, with particularly strong results in Miss Rate. Despite lacking the explicit semantic and topological annotations of pre-built HD maps and being subject to sensing noise, BEVTraj remains competitive, demonstrating that reliable trajectory prediction is achievable without HD map dependency under realistic conditions.

2) *Scene-Level Evaluation via Occupancy Prediction*: To complement per-agent trajectory metrics with a scene-level assessment, we additionally evaluate future occupancy prediction as a system-level proxy task. Unlike displacement-based errors that measure individual forecasts independently, occupancy forecasting directly reflects the spatial evolution of the entire scene and better captures transportation-system concerns such as space utilization, interaction feasibility, and potential conflict regions. For fair comparison with recent sensor-only end-to-end approaches that formulate motion prediction as BEV occupancy segmentation, we convert BEVTraj’s multi-agent trajectory outputs into occupancy grids through a deterministic post-processing step, without using any future ground-truth information. As summarized in Table III, BEVTraj achieves competitive performance under a realistic end-to-end setting where agent histories are inferred from detection and tracking results (E2E), and further demonstrates substantially stronger accuracy when ground-truth histories are provided (GT-hist). Despite not being explicitly trained with

TABLE IV
SCENARIO-WISE PERFORMANCE ON THE *nuScenes* VALIDATION SET. WE REPORT RESULTS ON FOUR CHALLENGING CONDITIONS: *rain*, *night*, *construction*, AND *heavy_traffic*.

Condition	Method	minADE ₅ ↓	minADE ₁₀ ↓	minFDE ₁ ↓	minFDE ₁₀ ↓	Miss Rate ₁₀ ↓
<i>rain</i>	Autobot	1.9784	1.1499	8.7597	2.2758	0.3133
	MTR	1.2967	1.0627	7.2870	2.3351	0.4357
	Wayformer	1.3827	0.9661	8.0107	2.1527	0.3793
	DeMo	1.2927	0.8345	6.4617	1.6804	0.2256
	BEVTraj (Ours)	1.4626	0.9464	8.3420	2.0262	0.2995
<i>night</i>	Autobot	1.9710	1.1554	8.9577	2.3311	0.3170
	MTR	1.4276	1.1298	7.7650	2.4510	0.4313
	Wayformer	1.3492	0.9828	7.7897	2.2732	0.3825
	DeMo	1.2812	0.8654	6.2776	1.7833	0.2202
	BEVTraj (Ours)	1.2870	0.9034	7.0542	1.9268	0.2201
<i>construction</i>	Autobot	1.9572	1.1795	8.7640	2.4068	0.3431
	MTR	1.2964	1.0554	7.1921	2.3023	0.4232
	Wayformer	1.3059	0.9564	7.7272	2.1423	0.3540
	DeMo	1.2952	0.8551	6.3589	1.7188	0.2371
	BEVTraj (Ours)	1.4480	0.8965	8.4993	1.8684	0.2750
<i>heavy_traffic</i>	Autobot	0.8487	0.7962	5.7484	2.0362	0.3208
	MTR	0.9042	0.8449	3.6851	2.0185	0.5094
	Wayformer	0.7669	0.6949	6.2221	2.0471	0.3774
	DeMo	0.6723	0.5962	2.8915	1.4073	0.1887
	BEVTraj (Ours)	0.8746	0.6621	5.6646	1.6686	0.3019

occupancy supervision, these results indicate that the proposed trajectory-centric modeling learns geometrically consistent and interaction-aware scene dynamics. Overall, the occupancy evaluation verifies that BEVTraj generalizes beyond agent-level forecasting and maintains coherent system-level scene prediction.

3) *Robustness under Challenging Driving Conditions*: To assess robustness under adverse driving conditions, we conduct a scenario-wise evaluation on the *nuScenes* validation set, including *rain*, *night*, *construction*, and *heavy_traffic*, where all subsets are consistently filtered using scenario metadata and evaluated with the same protocol and metrics as the full set (Table IV). We focus on the failure-oriented metric **Miss Rate**₁₀, which more directly reflects collapse-like prediction behavior. BEVTraj maintains consistently low failure rates across all subsets (0.22–0.30), achieving particularly strong robustness at *night* and remaining stable in complex scenes such as *construction* and *heavy_traffic*, where occlusions and dense interactions are prevalent. By contrast, map-based approaches rely on pre-built HD maps and are therefore largely unaffected by such adverse perception conditions. Overall, these results demonstrate that the proposed map-free design provides reliable and stable trajectory predictions across diverse and challenging environments.

D. Qualitative Results

To gain deeper insights into the prediction behavior of BEVTraj beyond quantitative metrics, we perform a qualitative study across diverse driving scenarios. This analysis aims to examine how effectively the model extracts motion-relevant scene context and surrounding agent cues from raw sensor inputs, and how these representations translate into consistent and plausible trajectory predictions.

1) *Qualitative Comparison of Trajectory Predictions*: As illustrated in Fig. 7, BEVTraj produces stable and lane-aligned future trajectories even under challenging conditions such as sharp curves and cluttered intersections. In contrast, baseline models frequently generate trajectories that drift into incorrect

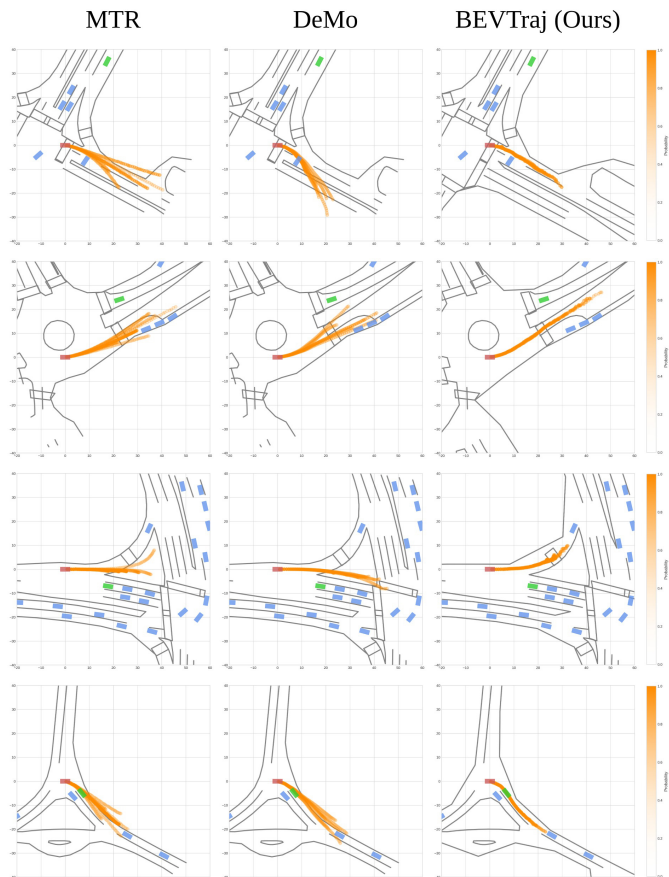


Fig. 7. Qualitative comparison in diverse driving scenarios. BEVTraj shows consistently accurate, lane-aligned predictions under complex conditions such as sharp turns and cluttered intersections, benefiting from directly leveraging raw sensor cues that are not available in map-based representations.

lanes or violate road boundaries, particularly in geometrically complex regions.

We attribute this difference primarily to the nature of the input representation. Vectorized HD maps provide compact and structured abstractions, but their coordinate-based representations are typically encoded directly by MLP-based networks, which may tend to weaken local spatial correlations and inevitably discard fine-grained spatial details present in raw sensor data. As a result, fine-grained cues such as road surface markings, free-space continuity, and subtle geometric boundaries are not explicitly preserved. In contrast, BEVTraj operates on a rasterized BEV representation constructed directly from sensors, which maintains continuous spatial structure and richer local geometry, allowing the model to better infer drivable areas and respect lane constraints.

These observations suggest that directly modeling dense sensor-derived features provides stronger geometric guidance for trajectory prediction, contributing to BEVTraj’s improved robustness in complex driving scenarios.

2) *Visualization of BEV Feature Representations*: To better understand why the BEV formulation provides stronger geometric guidance, we directly visualize the intermediate BEV features constructed from camera, LiDAR, and their fusion (Fig. 8). These visualizations reveal clear modality-specific

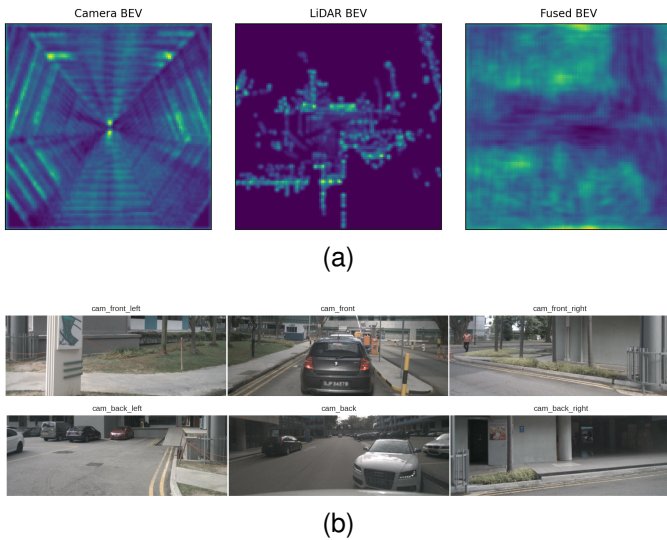


Fig. 8. Qualitative visualization of the BEV representation prior to trajectory reasoning. (a) Fused BEV feature representation constructed from multi-view cameras and LiDAR, where the right side corresponds to the ego vehicle’s forward direction. (b) Corresponding multi-view camera images used jointly with LiDAR to build the fused BEV representation.

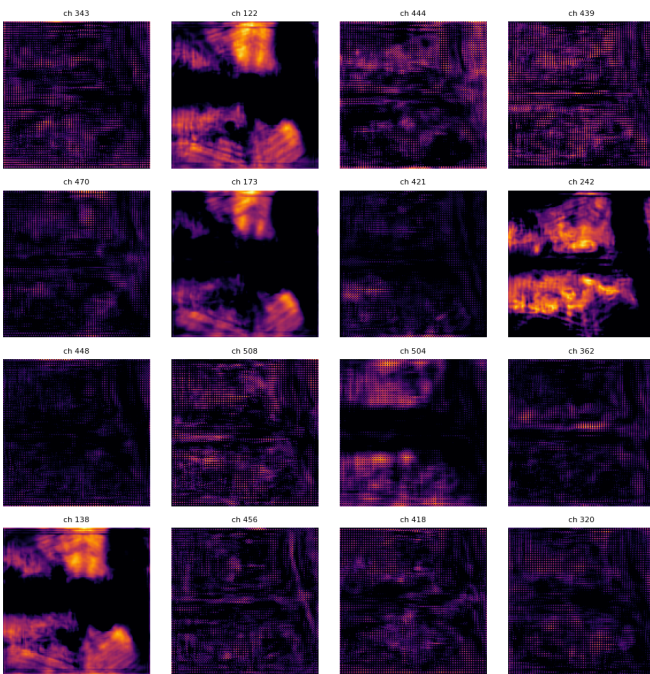


Fig. 9. Per-channel visualization of the fused BEV feature. Different channels exhibit distinct activation patterns, reflecting heterogeneous semantic and geometric information preserved in the fused BEV representation.

characteristics. Camera-derived BEV features tend to emphasize semantic and contextual cues, while LiDAR-derived features exhibit sharper geometric structures corresponding to road boundaries, obstacles, and free-space layouts.

The fused BEV feature is visualized via channel-wise max pooling, which aggregates heterogeneous activations into a single dense map and makes it difficult to interpret directly. A clearer picture emerges when we inspect the features on a per-channel basis (Fig. 9). Different channels exhibit markedly different activation patterns: some resemble geometry-dominant

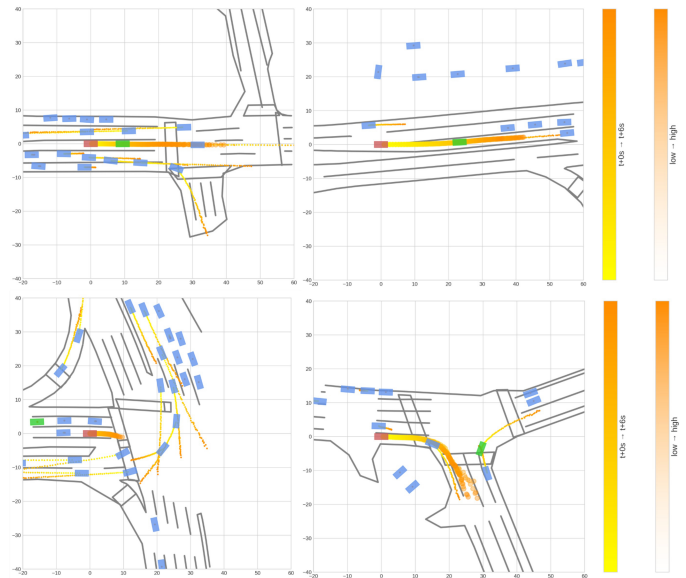


Fig. 10. Visualization of dense future prediction for surrounding agents.

structures similar to LiDAR features, while others reflect semantic activations akin to camera-based features. This heterogeneous structure suggests that the fused BEV representation implicitly preserves complementary semantic and geometric information across channels, providing rich scene cues that can be selectively exploited for downstream trajectory reasoning.

3) *Dense Scene-Level Motion Modeling*: Beyond predicting the designated target agent, BEVTraj explicitly accounts for the future motions of surrounding agents through dense future prediction [46]. During scene context encoding, the model predicts dense multi-agent futures over the BEV grid, enabling scene-level motion understanding that captures how nearby agents are expected to evolve over time.

As shown in Fig. 10, the resulting predictions exhibit coherent and consistent multi-agent patterns across the scene. This dense consideration of surrounding traffic provides informative interaction cues and contributes to more stable and interaction-aware target-agent predictions.

4) *Sparse Goal Candidates and Decoded Trajectories*: To illustrate how BEVTraj forms structured motion hypotheses prior to trajectory decoding, we visualize the outputs of the Sparse Goal Candidate Proposal (SGCP) module in Fig. 11. SGCP generates a compact and spatially diversified set of goal candidates that represent distinct high-level motion intents, enabling efficient hypothesis generation directly from BEV features without relying on predefined structures or hand-crafted sampling.

Each goal candidate is overlaid with its corresponding decoded trajectory, explicitly showing how sparse goals serve as anchors for multi-modal prediction. The decoder subsequently refines these anchors into temporally consistent motion forecasts, linking high-level goal reasoning with detailed trajectory generation.

5) *Layer-wise Evolution of Deformable Attention Geometry*: To illustrate how BEVTraj progressively refines future trajectories, we visualize the layer-wise evolution of reference



Fig. 11. Visualization of SGCP-proposed goals and their corresponding final trajectories. SGCP can generate a compact, spatially diversified set of goal candidates.

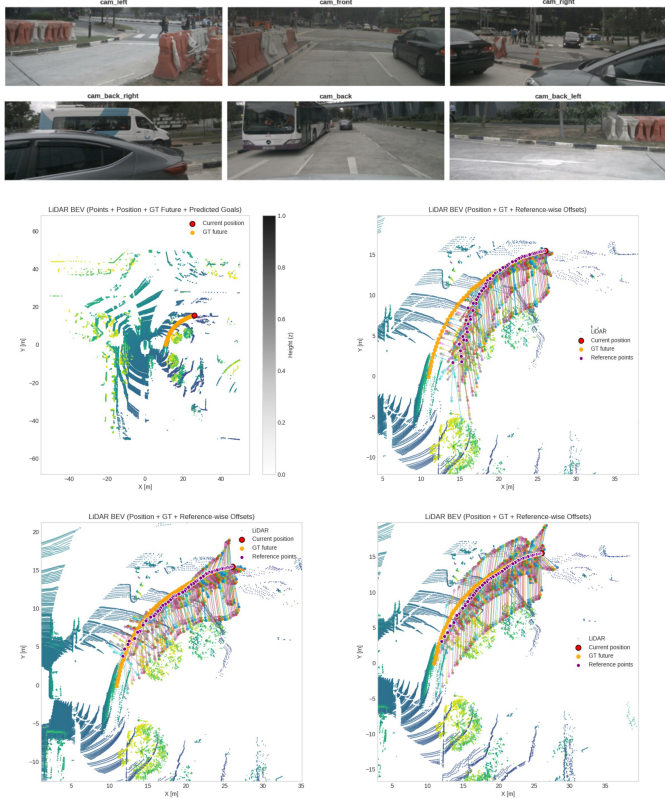


Fig. 12. Visualization of iterative reference point refinement in the Iterative Trajectory Refinement (ITR) module. The top panel shows the six camera images. The subsequent panel visualizes the predicted future trajectory as deformable-attention reference points, together with the corresponding sampling locations, overlaid with the ground-truth future trajectory in the ego-vehicle-centered coordinate frame.

points and sampling locations in the Iterative Trajectory Refinement (ITR) module in Fig. 12. Each layer updates future waypoint references, which subsequently guide deformable attention to aggregate scene features around the current motion hypotheses.

Across iterations, the sampling locations adaptively concentrate on regions that are most relevant to the predicted path,

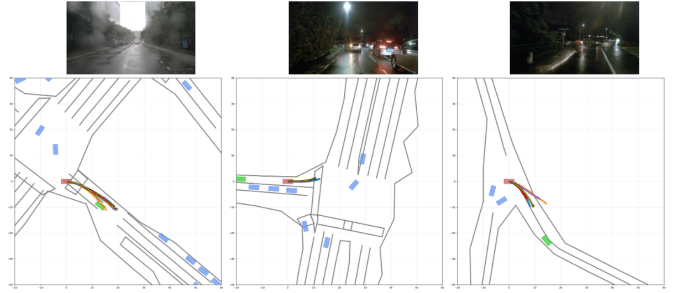


Fig. 13. Qualitative comparison of trajectory predictions under adverse visibility in nuScenes. Each column presents one representative case (rain/night). The top row shows the front-view camera image, and the bottom row overlays multi-modal trajectory predictions from different methods in the BEV space together with the ground truth. For each method, we visualize the highest-score trajectory among its multiple candidates.

TABLE V
ABLATION STUDY ON THE IMPACT OF DIFFERENT COMPONENTS.

Method	Pre-Encoder	SGCP	minADE ₅ ↓	minADE ₁₀ ↓	minFDE ₁ ↓	minFDE ₁₀ ↓	Miss Rate ↓
MTR	X	-	1.4204	1.1222	8.1122	2.4326	0.4443
	O	-	1.3718	1.1146	7.5796	2.3875	0.4156
BEVTraj	X	O	1.6501	1.0356	8.7623	2.3186	0.2852
	O	X	1.7060	1.0790	9.4390	2.4280	0.3603
	O	O	1.3953	0.9051	8.1975	1.8964	0.2783

yielding a coarse-to-fine refinement process. This dynamic receptive field enables agent-centric and motion-aware feature aggregation, allowing the model to progressively improve trajectory accuracy without relying on explicit HD-map priors.

6) *Robustness under Adverse Visibility Conditions*: Finally, to complement the representation and mechanism-oriented analyses above, we evaluate the robustness of BEVTraj under adverse visibility conditions such as *rain* and *night*, where visibility is degraded by raindrops, reflections, and low illumination. Fig. 13 provides qualitative comparisons with multiple representative methods, offering a direct visual reference of trajectory forecasts under these challenging scenarios, particularly during geometry-sensitive maneuvers such as turning and lane-following. In the shown examples, BEVTraj maintains trajectories that remain well aligned with the local road geometry and closely follow the ground-truth motion, demonstrating stable lane-consistent behavior despite weakened visual cues. These results further confirm that BEVTraj produces reliable and usable predictions even under degraded-visibility conditions.

E. Ablation Study

We conduct comprehensive ablation studies to analyze the design of BEVTraj from three aspects: the contribution of core architectural components, the scalability and runtime trade-offs with respect to the number of modes, and key design choices in the decoder. Unless otherwise specified, all experimental settings follow Section IV-A.

1) *Component-wise Ablation*: We first evaluate the contribution of the Pre-Encoder and SGCP. As shown in Table V, introducing the Pre-Encoder consistently improves overall accuracy—particularly minFDE—by modeling temporal dynamics and inter-agent interactions prior to temporal compression, while SGCP further enhances endpoint prediction

TABLE VI
ABLATION STUDY ON THE NUMBER OF PREDICTION MODES.

Num Modes	minADE ₅ ↓	minADE ₁₀ ↓	minFDE ₁ ↓	minFDE ₁₀ ↓	Miss Rate↓
10 (default)	1.3953	0.9051	8.1975	1.8964	0.2783
64	1.6070	1.0132	9.1218	2.1571	0.2667

TABLE VII
RUNTIME OF THE ITERATIVE TRAJECTORY DECODER UNDER DIFFERENT NUMBERS OF MODES. INCREASING THE NUMBER OF MODES SUBSTANTIALLY INCREASES LATENCY, ESPECIALLY WITH VANILLA ATTENTION.

Configuration	Runtime (ms)
Mode 10 (deform attn)	19.30
Mode 10 (vanilla attn)	27.42
Mode 16 (deform attn)	19.35
Mode 64 (deform attn)	26.41
Mode 64 (vanilla attn)	85.85
Mode 128 (deform attn)	43.83
Mode 256 (deform attn)	83.64

by generating intention-aware goal candidates that provide reliable spatial anchors for downstream decoding. These results confirm that early temporal–social modeling and explicit goal proposal are both critical for robust trajectory forecasting.

2) *Mode Scalability and Runtime Analysis*: To validate that a small set of carefully selected, scene-adaptive goals can achieve strong performance without brute-force mode scaling, we analyze the effect of increasing the number of trajectory modes with learning-rate tuning and extended training. As shown in Table VI, adding more modes degrades most evaluation metrics without improving reliability. This behavior is consistent with prior findings: Shi et al. [46] demonstrate that when queries are not anchored to predefined intentions, increasing the number of modes results in unstable optimization and arbitrary mode switching. Taken together, these results indicate that a sparse set of scene-adaptive goals is both sufficient and more effective than brute-force mode scaling.

Beyond accuracy, increasing the number of modes also reduces inference efficiency, as decoder runtime grows substantially with the number of modes (Table VII). Although deformable attention scales more favorably than global attention, naive mode scaling remains computationally inefficient. Overall, these results show that post-hoc selection from many modes is ill-suited for anchor-free designs such as BEVTraj, motivating SGCP to instead predict a small set of high-quality, scene-adaptive goals that better balance accuracy and efficiency.

3) *Design Choices in the Decoder*: We analyze key design choices in the decoder, focusing on the coordinate-system formulation for reference point prediction and the attention mechanism used for BEV feature aggregation in SGCP. As shown in Table VIII, using either ego-centric or target-centric coordinates alone leads to suboptimal performance: ego-centric modeling relies on unnormalized absolute positions, while target-centric modeling introduces structural misalignment with ego-centric BEV features. In contrast, jointly encoding both coordinate systems consistently achieves the best performance across all metrics, indicating that effective

TABLE VIII
ABLATION STUDY ON DIFFERENT COORDINATE-SYSTEM CONFIGURATIONS FOR DECODER-SIDE REFERENCE POINT PREDICTION IN SGCP. THE BASELINE CORRESPONDS TO THE ORIGINAL SGCP DESIGN PRIOR TO THE PROPOSED REVISION.

Configuration	minADE ₅ ↓	minADE ₁₀ ↓	minFDE ₁ ↓	minFDE ₁₀ ↓	Miss Rate↓
baseline	1.4556	0.9438	8.4384	2.0527	0.3082
ego-centric	1.3978	0.9056	8.4517	2.0267	0.2952
target-centric	1.4528	0.9444	8.0119	2.0069	0.2875
ec & tc	1.3953	0.9051	8.1975	1.8964	0.2783

TABLE IX
ABLATION STUDY ON EXPLICIT POSITIONAL KEY CONSTRUCTION FOR DEFORMABLE ATTENTION IN THE ITP/ITR STAGES.

Pos Key	minADE ₅ ↓	minADE ₁₀ ↓	minFDE ₁ ↓	minFDE ₁₀ ↓	Miss Rate↓
X	1.4213	0.9377	9.8164	1.9349	0.2685
O	1.3953	0.9051	8.1975	1.8964	0.2783

reference point prediction requires normalized relative motion cues together with spatial alignment to the BEV frame.

We further revisit the deformable attention formulation used in the decoder. Standard deformable attention does not explicitly encode positional information in keys, which limits its ability to reason about geometric constraints in BEV space. By explicitly constructing positional keys and decomposing attention into content and positional components, the decoder achieves lower displacement errors, as shown in Table IX. This result demonstrates improved spatial reasoning and goal localization, validating the effectiveness of explicit positional key modeling for trajectory prediction.

F. Discussion

While the previous sections focus on benchmark-level performance and component analysis, we further examine how BEVTraj behaves under practical deployment conditions. In this section, we analyze scene-level multi-agent consistency, sensing-range limitations, and ego-motion forecasting to better understand the system-level implications of the proposed design.

1) Multi-agent Trajectory Prediction:

a) *Method*: To model the future behaviors of multiple interacting agents, we construct S scene-level *joint future predictions*, each formed by selecting one of the modes per agent and combining them into a joint world [68]. A naive strategy is to independently choose the highest-probability mode for each agent. However, such independent selection over-relies on model confidence and often collapses the multi-modal hypothesis set, reducing diversity. Moreover, it fails to enforce cross-agent compatibility, potentially yielding interaction-infeasible joint futures. Therefore, we formulate joint-world construction as a constrained assignment problem with interaction-aware costs.

For each agent i , we assign its K modes to the S worlds by minimizing a weighted cost:

$$C_i(s, k) = w_{\text{prob}} c_{\text{prob}}(i, k) + w_{\text{pair}} c_{\text{pair}}(i, k; \mathcal{T}_s) + w_{\text{ego}} c_{\text{ego}}(i, k) + w_{\text{reg}} c_{\text{reg}}(i, k), \quad (6)$$

where $c_{\text{prob}}(i, k) = -\log p_{i,k}$ and $c_{\text{pair}}(i, k; \mathcal{T}_s)$ penalizes sustained close proximity to trajectories already cached in

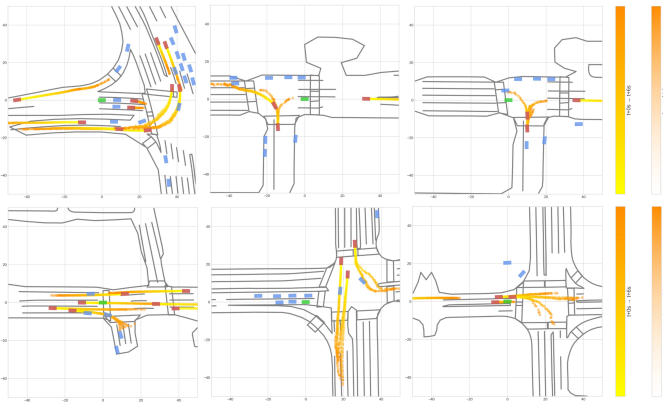


Fig. 14. Visualization of BEVTraj’s multi-agent predictions for several agents that exhibit strong interaction relevance with the ego-vehicle. Red indicates the target agents, and green indicates the ego vehicle. For compact presentation, multi-worlds predictions are aggregated into a single visualization, and only the top three most probable modes are shown.

world s (distance threshold with an L -consecutive criterion); c_{ego} is optional and c_{reg} is a lightweight motion regularizer.

We then solve the resulting minimum-cost one-to-one assignment using the Hungarian algorithm, with \mathcal{T}_s updated sequentially so that c_{pair} accounts for agents already assigned to each world. This produces diverse joint worlds that better respect interaction feasibility for system-level evaluation.

b) System-level Multi-agent Evaluation: We run inference for all agents in a scene, assemble them into $S=6$ joint multi-worlds using our matching procedure, and evaluate them as K scene-level predictions under the Argoverse 2 [69] protocol using its standard system-level metrics (avgMinADE, avgMinFDE, actorMR, and ActorCR). In addition, we introduce **NodeCR**, a node-level collision rate that measures the fraction of actor–timestep nodes whose pairwise distance violates a threshold for at least L consecutive timesteps (default $d_{\text{th}}=1.6$ m, $L=2$), capturing sustained overlap risk.

c) Analysis: Fig. 14 shows qualitative examples of BEVTraj’s multi-agent trajectory predictions. Although BEVTraj operates without HD-map priors, the proposed Matching post-processing substantially improves the safety of the assembled joint futures, yielding the lowest collision-related rates after Matching (NodeCR= 0.0000, ActorCR= 0.0002) and the lowest miss rate (ActorMR= 0.4178) in Table X, outperforming HD-map-based baselines. Here, ActorCR counts an actor as collided if its minimum distance to any other actor falls below 1.0 m at any future timestep, while NodeCR measures sustained overlap risk as the fraction of actor–timestep nodes that violate a distance threshold for at least L consecutive timesteps (default $d_{\text{th}}=1.6$ m, $L=2$).

2) Effect of Map Range on Prediction Performance: As discussed in Section IV-C, real-time HD map construction is inherently limited by the sensor’s perceptual range. To analyze how this constraint affects prediction performance, we evaluated HD map-based models under varying map ranges (Tables XI and XII). Across most models and metrics, expanding the spatial range improves performance, confirming that broader contextual information benefits trajectory prediction. However, the gains are not uniform across architectures, and

TABLE X
PERFORMANCE COMPARISON UNDER THE MULTI-WORLD PREDICTION EVALUATION PROTOCOL ON THE *nuScenes* VALIDATION SET (LOWER IS BETTER).

Model	AvgMinADE \downarrow	AvgMinFDE \downarrow	ActorMR \downarrow	NodeCR \downarrow	ActorCR \downarrow
Autobot	2.6421	6.4028	0.7648	0.0002	0.0022
MTR	2.1352	5.4476	0.7229	0.0005	0.0030
Wayformer	2.1675	5.7544	0.7537	0.0001	0.0018
DEMO	1.8843	4.8902	0.6864	0.0002	0.0025
BEVTraj (Ours)	1.9285	4.9791	0.4178	0.0000	0.0002

TABLE XI
PERFORMANCE COMPARISON OF HD MAP-BASED MODELS ON THE *nuScenes* VALIDATION SET. THE NUMBER IN PARENTHESES INDICATES THE SPATIAL RANGE (IN METERS) OF THE INPUT HD MAP (*i.e.*, 30M, 50M, 100M).

Method	minADE \downarrow	minADE \downarrow	minFDE \downarrow	minFDE \downarrow	Miss Rate \downarrow
Autobot (30)	1.9407	1.1969	9.9123	2.4823	0.4023
Autobot (50)	1.9566	1.1649	8.8171	2.3294	0.3229
Autobot (100)	1.8475	1.1100	9.0446	2.1356	0.3190
MTR (30)	1.3228	1.0547	7.2409	2.3198	0.4291
MTR (50)	1.2926	1.0446	7.2689	2.2840	0.4240
MTR (100)	1.2722	1.0332	7.3652	2.2170	0.4007
Wayformer (30)	1.3983	1.0226	8.0459	2.3181	0.3903
Wayformer (50)	1.4034	0.9877	7.9707	2.2483	0.3868
Wayformer (100)	1.4166	0.9620	7.6164	2.1658	0.3552
DeMo (30)	1.3669	0.9575	6.9147	1.9255	0.2886
DeMo (50)	1.3137	1.0424	7.1679	2.1806	0.3399
DeMo (100)	1.3518	0.9254	6.9370	1.8536	0.2833

TABLE XII
PERFORMANCE COMPARISON OF HD MAP-BASED MODELS ON THE *Argoverse 2 Sensor* VALIDATION SET. THE NUMBER IN PARENTHESES INDICATES THE SPATIAL RANGE (IN METERS) OF THE INPUT HD MAP (*i.e.*, 30M, 50M, 100M).

Method	minADE \downarrow	minADE \downarrow	minFDE \downarrow	minFDE \downarrow	Miss Rate \downarrow
Autobot (30)	1.3426	0.8128	7.5449	1.8431	0.2470
Autobot (50)	1.3284	0.7430	6.9975	1.6861	0.2136
Autobot (100)	1.3052	0.7370	6.8554	1.6304	0.1977
MTR (30)	0.9558	0.8055	5.8315	2.0128	0.3221
MTR (50)	0.9243	0.7944	5.8264	1.9926	0.3361
MTR (100)	0.9299	0.7961	5.9988	2.0115	0.3237
Wayformer (30)	1.0499	0.7009	6.2962	1.7431	0.2344
Wayformer (50)	1.0454	0.6721	6.2511	1.6775	0.2181
Wayformer (100)	1.0268	0.7122	6.0104	1.8444	0.2521
DeMo (30)	0.9142	0.6046	5.8348	1.3308	0.1692
DeMo (50)	0.8528	0.6426	5.2801	1.4964	0.1976
DeMo (100)	0.8133	0.5107	4.9291	1.2306	0.1455

some models fail to effectively exploit extended context, occasionally showing limited or degraded performance. This observation highlights that the usefulness of additional spatial information depends on how well a model integrates contextual cues. In contrast, BEVTraj is explicitly designed to aggregate informative regions through deformable attention, suggesting that it can more effectively capitalize on expanded sensing coverage. Consequently, extending the perceptual range—through improved sensors or cooperative infrastructure such as V2X—may further enhance its prediction accuracy.

3) Ego-Vehicle Trajectory Prediction: In addition to predicting surrounding agents, we evaluated the model’s ability to forecast the ego vehicle’s future trajectory. As shown in Table XIII, our method achieves comparable or slightly improved performance over HD map-based baselines. Notably, ego trajectory prediction tends to be more reliable than

TABLE XIII

EGO-VEHICLE TRAJECTORY FORECASTING RESULTS ON THE VALIDATION SET OF THE *nuScenes Dataset*. BEVTRAJ ACHIEVES COMPARABLE PERFORMANCE TO HD MAP-BASED BASELINES UNDER THE SAME SPATIAL COVERAGE CONSTRAINT.

Method	minADE ₅ ↓	minADE ₁₀ ↓	minFDE ₁ ↓	minFDE ₁₀ ↓	Miss Rate ↓
Autobot	1.1059	0.9432	6.9950	2.1440	0.3313
MTR	0.9528	0.8958	6.0512	2.0596	0.3649
Wayformer	1.0501	0.6827	6.5616	1.4936	0.2131
DeMo	1.0720	0.7986	5.6852	1.8206	0.2490
BEVTraj (Ours)	1.1694	0.6751	6.3221	1.3170	0.1374

surrounding-agent prediction. This advantage stems from the use of onboard sensor data, which provides rich, real-time cues that are directly coupled with the ego vehicle’s own motion and immediate environment. Such ego-centric observations offer stronger behavioral signals than those available for other agents, enabling more accurate and stable ego trajectory forecasting.

Furthermore, although BEVTraj is primarily designed for trajectory prediction, its sensor-driven BEV representation and interaction-aware modeling are conceptually aligned with the requirements of motion planning. These properties suggest that the proposed framework can offer useful insights and transferable components for planning research, supporting closer integration between perception, prediction, and decision-making.

V. CONCLUSION

In this paper, we introduced Bird’s-Eye View Trajectory Prediction (BEVTraj), a novel end-to-end framework that eliminates dependence on pre-built HD maps by directly leveraging real-time sensor data. BEVTraj effectively captures dynamic environmental changes while maintaining high prediction accuracy. It utilizes a BEV-based representation to encode spatial and contextual information, and employs deformable attention to selectively extract salient features from dense BEV inputs, enabling accurate and consistent trajectory prediction.

Moreover, the proposed Sparse Goal Candidate Proposal (SGCP) module improves efficiency by removing the need for post-processing operations. Extensive experiments demonstrate that BEVTraj achieves performance competitive with HD map-based methods, while offering enhanced adaptability across diverse driving scenarios. These findings validate the feasibility of map-free trajectory prediction and highlight BEVTraj’s potential as a scalable and flexible solution for autonomous driving.

Beyond autonomous driving, the techniques developed in this work are not limited to a single application domain but can also be extended to broader areas, such as surveillance systems—where monitoring vehicle and human activities is critical for safety [70]–[75]—and robotics, where accurate trajectory prediction is essential for tasks such as human–robot interaction and navigation in dynamic environments [76].

ACKNOWLEDGMENTS

This work was supported by Artificial intelligence industrial convergence cluster development project funded by the Ministry of Science and ICT(MSIT, Korea) & Gwangju

Metropolitan City and the National Research Foundation of Korea (NRF) grant funded by the Korea government (MSIT). (No. 2020R1A2C1102767)

REFERENCES

- [1] Y. Li, S. Dalhatu, and C. Yuan, “Analysing freeway diverging risks using high-resolution trajectory data based on conflict prediction models,” *Transportation safety and environment*, vol. 6, no. 1, p. tdad002, 2024.
- [2] X. Chen, S. Wu, C. Shi, Y. Huang, Y. Yang, R. Ke, and J. Zhao, “Sensing data supported traffic flow prediction via denoising schemes and ann: A comparison,” *IEEE Sensors Journal*, vol. 20, no. 23, pp. 14 317–14 328, 2020.
- [3] X. Chen, Z. Li, Y. Yang, L. Qi, and R. Ke, “High-resolution vehicle trajectory extraction and denoising from aerial videos,” *IEEE Transactions on Intelligent Transportation Systems*, vol. 22, no. 5, pp. 3190–3202, 2020.
- [4] Q. Li, Y. Wang, Y. Wang, and H. Zhao, “Hdmapnet: An online hd map construction and evaluation framework,” in *2022 International Conference on Robotics and Automation (ICRA)*. IEEE, 2022, pp. 4628–4634.
- [5] B. Liao, S. Chen, X. Wang, T. Cheng, Q. Zhang, W. Liu, and C. Huang, “Maptr: Structured modeling and learning for online vectorized hd map construction,” *arXiv preprint arXiv:2208.14437*, 2022.
- [6] S. Choi, J. Kim, H. Shin, and J. W. Choi, “Mask2map: Vectorized hd map construction using bird’s eye view segmentation masks,” in *European Conference on Computer Vision*. Springer, 2024, pp. 19–36.
- [7] A. Vaswani, “Attention is all you need,” *Advances in Neural Information Processing Systems*, 2017.
- [8] Z. Liu, Y. Lin, Y. Cao, H. Hu, Y. Wei, Z. Zhang, S. Lin, and B. Guo, “Swin transformer: Hierarchical vision transformer using shifted windows,” in *Proceedings of the IEEE/CVF international conference on computer vision*, 2021, pp. 10 012–10 022.
- [9] X. Zhu, W. Su, L. Lu, B. Li, X. Wang, and J. Dai, “Deformable detr: Deformable transformers for end-to-end object detection,” *arXiv preprint arXiv:2010.04159*, 2020.
- [10] Y. Biktairov, M. Stebelev, I. Rudenko, O. Shliashko, and B. Yangel, “Prank: motion prediction based on ranking,” *Advances in neural information processing systems*, vol. 33, pp. 2553–2563, 2020.
- [11] S. Casas, C. Gulino, R. Liao, and R. Urtasun, “Spagmn: Spatially-aware graph neural networks for relational behavior forecasting from sensor data,” in *2020 IEEE International Conference on Robotics and Automation (ICRA)*. IEEE, 2020, pp. 9491–9497.
- [12] S. Casas, A. Sadat, and R. Urtasun, “Mp3: A unified model to map, perceive, predict and plan,” in *Proceedings of the IEEE/CVF Conference on Computer Vision and Pattern Recognition*, 2021, pp. 14 403–14 412.
- [13] N. Djuric, V. Radosavljevic, H. Cui, T. Nguyen, F.-C. Chou, T.-H. Lin, N. Singh, and J. Schneider, “Uncertainty-aware short-term motion prediction of traffic actors for autonomous driving,” in *Proceedings of the IEEE/CVF Winter Conference on Applications of Computer Vision*, 2020, pp. 2095–2104.
- [14] F. Marchetti, F. Becattini, L. Seidenari, and A. D. Bimbo, “Mantra: Memory augmented networks for multiple trajectory prediction,” in *Proceedings of the IEEE/CVF conference on computer vision and pattern recognition*, 2020, pp. 7143–7152.
- [15] J. Gao, C. Sun, H. Zhao, Y. Shen, D. Anguelov, C. Li, and C. Schmid, “Vectormet: Encoding hd maps and agent dynamics from vectorized representation,” in *Proceedings of the IEEE/CVF conference on computer vision and pattern recognition*, 2020, pp. 11 525–11 533.
- [16] M. Liang, B. Yang, R. Hu, Y. Chen, R. Liao, S. Feng, and R. Urtasun, “Learning lane graph representations for motion forecasting,” in *European Conference on Computer Vision*. Springer, 2020, pp. 541–556.
- [17] L. Tabelini, R. Berriel, T. M. Paixao, C. Badue, A. F. De Souza, and T. Oliveira-Santos, “Keep your eyes on the lane: Real-time attention-guided lane detection,” in *Proceedings of the IEEE/CVF conference on computer vision and pattern recognition*, 2021, pp. 294–302.
- [18] H. Zhao, J. Gao, T. Lan, C. Sun, B. Sapp, B. Varadarajan, Y. Shen, Y. Shen, Y. Chai, C. Schmid *et al.*, “Tnt: Target-driven trajectory prediction,” in *Conference on robot learning*. PMLR, 2021, pp. 895–904.
- [19] N. Nayakanti, R. Al-Rfou, A. Zhou, K. Goel, K. S. Refaat, and B. Sapp, “Wayformer: Motion forecasting via simple & efficient attention networks,” *arXiv preprint arXiv:2207.05844*, 2022.

- [20] B. Zhang, N. Song, and L. Zhang, "Decoupling motion forecasting into directional intentions and dynamic states," *arXiv preprint arXiv:2410.05982*, 2024.
- [21] S. Shi, L. Jiang, D. Dai, and B. Schiele, "Motion transformer with global intention localization and local movement refinement," *Advances in Neural Information Processing Systems*, vol. 35, pp. 6531–6543, 2022.
- [22] J. Ngiam, B. Caine, V. Vasudevan, Z. Zhang, H.-T. L. Chiang, J. Ling, R. Roelofs, A. Bewley, C. Liu, A. Venugopal *et al.*, "Scene transformer: A unified architecture for predicting multiple agent trajectories," *arXiv preprint arXiv:2106.08417*, 2021.
- [23] Z. Zhou, J. Wang, Y.-H. Li, and Y.-K. Huang, "Query-centric trajectory prediction," in *Proceedings of the IEEE/CVF conference on computer vision and pattern recognition*, 2023, pp. 17 863–17 873.
- [24] M. Pei, S. Shi, X. Chen, X. Liu, and S. Shen, "Foresight in motion: Reinforcing trajectory prediction with reward heuristics," in *Proceedings of the IEEE/CVF International Conference on Computer Vision*, 2025, pp. 28 303–28 312.
- [25] J. Schmidt, J. Jordan, F. Gritschneider, and K. Dietmayer, "Crat-pred: Vehicle trajectory prediction with crystal graph convolutional neural networks and multi-head self-attention," in *2022 International Conference on Robotics and Automation (ICRA)*. IEEE, 2022, pp. 7799–7805.
- [26] J. Xiang, Z. Nan, Z. Song, J. Huang, and L. Li, "Map-free trajectory prediction in traffic with multi-level spatial-temporal modeling," *IEEE Transactions on Intelligent Vehicles*, vol. 9, no. 2, pp. 3258–3270, 2023.
- [27] Y. Hou, X. Zhang, X. Cao, Z. Lu, and X. Yuan, "Vehicle trajectory prediction model for map-free scenes using the spatio-temporal attentional mechanism," *IEEE Internet of Things Journal*, 2024.
- [28] Y. Ren, L. Liu, Z. Lan, Z. Cui, and H. Yu, "Mlb-traj: Map-free trajectory prediction with local behavior query for autonomous driving," *IEEE Internet of Things Journal*, 2025.
- [29] Y. Yuan and K. Kitani, "Dlow: Diversifying latent flows for diverse human motion prediction," in *European Conference on Computer Vision*. Springer, 2020, pp. 346–364.
- [30] Y. Yuan, X. Weng, Y. Ou, and K. M. Kitani, "Agentformer: Agent-aware transformers for socio-temporal multi-agent forecasting," in *Proceedings of the IEEE/CVF international conference on computer vision*, 2021, pp. 9813–9823.
- [31] H. Cheng, M. Liu, L. Chen, H. Broszio, M. Sester, and M. Y. Yang, "Gatraj: A graph-and attention-based multi-agent trajectory prediction model," *ISPRS Journal of Photogrammetry and Remote Sensing*, vol. 205, pp. 163–175, 2023.
- [32] J. Phillion and S. Fidler, "Lift, splat, shoot: Encoding images from arbitrary camera rigs by implicitly unprojecting to 3d," in *European conference on computer vision*. Springer, 2020, pp. 194–210.
- [33] J. Huang, G. Huang, Z. Zhu, Y. Ye, and D. Du, "Bevdet: High-performance multi-camera 3d object detection in bird-eye-view," *arXiv preprint arXiv:2112.11790*, 2021.
- [34] Y. Li, Z. Ge, G. Yu, J. Yang, Z. Wang, Y. Shi, J. Sun, and Z. Li, "Bevdepth: Acquisition of reliable depth for multi-view 3d object detection," in *Proceedings of the AAAI conference on artificial intelligence*, vol. 37, no. 2, 2023, pp. 1477–1485.
- [35] Z. Li, W. Wang, H. Li, E. Xie, C. Sima, T. Lu, Q. Yu, and J. Dai, "Bevformer: learning bird's-eye-view representation from lidar-camera via spatiotemporal transformers," *IEEE Transactions on Pattern Analysis and Machine Intelligence*, 2024.
- [36] C. Yang, Y. Chen, H. Tian, C. Tao, X. Zhu, Z. Zhang, G. Huang, H. Li, Y. Qiao, L. Lu *et al.*, "Bevformer v2: Adapting modern image backbones to bird's-eye-view recognition via perspective supervision," in *Proceedings of the IEEE/CVF conference on computer vision and pattern recognition*, 2023, pp. 17 830–17 839.
- [37] J. Lu, Z. Zhou, X. Zhu, H. Xu, and L. Zhang, "Learning ego 3d representation as ray tracing," in *European conference on computer vision*. Springer, 2022, pp. 129–144.
- [38] Z. Lin, Z. Liu, Z. Xia, X. Wang, Y. Wang, S. Qi, Y. Dong, N. Dong, L. Zhang, and C. Zhu, "Rcbevdet: Radar-camera fusion in bird's eye view for 3d object detection," in *Proceedings of the IEEE/CVF Conference on Computer Vision and Pattern Recognition*, 2024, pp. 14 928–14 937.
- [39] Z. Lin, Z. Liu, Y. Wang, L. Zhang, and C. Zhu, "Rcbevdet++: toward high-accuracy radar-camera fusion 3d perception network," *arXiv preprint arXiv:2409.04979*, 2024.
- [40] L. Hou, S. E. Li, B. Yang, Z. Wang, and K. Nakano, "Integrated graphical representation of highway scenarios to improve trajectory prediction of surrounding vehicles," *IEEE Transactions on Intelligent Vehicles*, vol. 8, no. 2, pp. 1638–1651, 2022.
- [41] J. Hong, B. Sapp, and J. Philbin, "Rules of the road: Predicting driving behavior with a convolutional model of semantic interactions," in *Proceedings of the IEEE/CVF Conference on Computer Vision and Pattern Recognition*, 2019, pp. 8454–8462.
- [42] L. Li, X. Wang, D. Yang, Y. Ju, Z. Zhang, and J. Lian, "Real-time heterogeneous road-agents trajectory prediction using hierarchical convolutional networks and multi-task learning," *IEEE Transactions on Intelligent Vehicles*, vol. 9, no. 2, pp. 4055–4069, 2023.
- [43] A. Hu, Z. Murez, N. Mohan, S. Dudas, J. Hawke, V. Badrinarayanan, R. Cipolla, and A. Kendall, "Fiery: Future instance prediction in bird's-eye view from surround monocular cameras," in *Proceedings of the IEEE/CVF International Conference on Computer Vision*, 2021, pp. 15 273–15 282.
- [44] Y. Zhang, Z. Zhu, W. Zheng, J. Huang, G. Huang, J. Zhou, and J. Lu, "Beverse: Unified perception and prediction in birds-eye-view for vision-centric autonomous driving," *arXiv preprint arXiv:2205.09743*, 2022.
- [45] S. Fang, Z. Wang, Y. Zhong, J. Ge, and S. Chen, "Tbp-former: Learning temporal bird's-eye-view pyramid for joint perception and prediction in vision-centric autonomous driving," in *Proceedings of the IEEE/CVF conference on computer vision and pattern recognition*, 2023, pp. 1368–1378.
- [46] S. Shi, L. Jiang, D. Dai, and B. Schiele, "Motion transformer with global intention localization and local movement refinement," *Advances in Neural Information Processing Systems*, vol. 35, pp. 6531–6543, 2022.
- [47] C. R. Qi, H. Su, K. Mo, and L. J. Guibas, "Pointnet: Deep learning on point sets for 3d classification and segmentation," in *Proceedings of the IEEE conference on computer vision and pattern recognition*, 2017, pp. 652–660.
- [48] Z. Liu, H. Tang, A. Amini, X. Yang, H. Mao, D. L. Rus, and S. Han, "Bevfusion: Multi-task multi-sensor fusion with unified bird's-eye view representation," in *2023 IEEE international conference on robotics and automation (ICRA)*. IEEE, 2023, pp. 2774–2781.
- [49] J. Phillion and S. Fidler, "Lift, splat, shoot: Encoding images from arbitrary camera rigs by implicitly unprojecting to 3d," in *Computer Vision—ECCV 2020: 16th European Conference, Glasgow, UK, August 23–28, 2020, Proceedings, Part XIV 16*. Springer, 2020, pp. 194–210.
- [50] Z. Li, W. Wang, H. Li, E. Xie, C. Sima, T. Lu, Q. Yu, and J. Dai, "Bevformer: Learning bird's-eye-view representation from lidar-camera via spatiotemporal transformers," *IEEE Transactions on Pattern Analysis and Machine Intelligence*, 2024.
- [51] R. Girgis, F. Golemo, F. Codevilla, M. Weiss, J. A. D'Souza, S. E. Kahou, F. Heide, and C. Pal, "Latent variable sequential set transformers for joint multi-agent motion prediction," *arXiv preprint arXiv:2104.00563*, 2021.
- [52] S. Liu, F. Li, H. Zhang, X. Yang, X. Qi, H. Su, J. Zhu, and L. Zhang, "Dab-detr: Dynamic anchor boxes are better queries for detr," *arXiv preprint arXiv:2201.12329*, 2022.
- [53] J. Gu, C. Sun, and H. Zhao, "Densetnet: End-to-end trajectory prediction from dense goal sets," in *Proceedings of the IEEE/CVF International Conference on Computer Vision*, 2021, pp. 15 303–15 312.
- [54] E. Perez, F. Strub, H. De Vries, V. Dumoulin, and A. Courville, "Film: Visual reasoning with a general conditioning layer," in *Proceedings of the AAAI conference on artificial intelligence*, vol. 32, no. 1, 2018.
- [55] D. Meng, X. Chen, Z. Fan, G. Zeng, H. Li, Y. Yuan, L. Sun, and J. Wang, "Conditional detr for fast training convergence," in *Proceedings of the IEEE/CVF international conference on computer vision*, 2021, pp. 3651–3660.
- [56] H. Zhang, F. Li, S. Liu, L. Zhang, H. Su, J. Zhu, L. M. Ni, and H.-Y. Shum, "Dino: Detr with improved denoising anchor boxes for end-to-end object detection," *arXiv preprint arXiv:2203.03605*, 2022.
- [57] M. Ye, T. Cao, and Q. Chen, "Tpcn: Temporal point cloud networks for motion forecasting," in *Proceedings of the IEEE/CVF Conference on Computer Vision and Pattern Recognition*, 2021, pp. 11 318–11 327.
- [58] H. Caesar, V. Bankiti, A. H. Lang, S. Vora, V. E. Liong, Q. Xu, A. Krishnan, Y. Pan, G. Baldan, and O. Beijbom, "nuscenes: A multimodal dataset for autonomous driving," in *Proceedings of the IEEE/CVF conference on computer vision and pattern recognition*, 2020, pp. 11 621–11 631.
- [59] B. Wilson, W. Qi, T. Agarwal, J. Lambert, J. Singh, S. Khandelwal, B. Pan, R. Kumar, A. Hartnett, J. K. Pontes *et al.*, "Argoverse 2: Next generation datasets for self-driving perception and forecasting," *arXiv preprint arXiv:2301.00493*, 2023.
- [60] L. Feng, M. Bahari, K. M. B. Amor, É. Zablocki, M. Cord, and A. Alahi, "Unitraj: A unified framework for scalable vehicle trajectory prediction," in *European Conference on Computer Vision*. Springer, 2024, pp. 106–123.
- [61] Y. Zhang, Z. Zhu, W. Zheng, J. Huang, G. Huang, J. Zhou, and J. Lu, "Beverse: Unified perception and prediction in birds-eye-view for vision-centric autonomous driving," *arXiv preprint arXiv:2205.09743*, 2022.

[62] A. Hu, Z. Murez, N. Mohan, S. Dudas, J. Hawke, V. Badrinarayanan, R. Cipolla, and A. Kendall, "Fiery: Future instance prediction in bird's-eye view from surround monocular cameras," in *Proceedings of the IEEE/CVF International Conference on Computer Vision*, 2021, pp. 15 273–15 282.

[63] A. K. Akan and F. Güney, "Stretchbev: Stretching future instance prediction spatially and temporally," in *European Conference on Computer Vision*. Springer, 2022, pp. 444–460.

[64] S. Hu, L. Chen, P. Wu, H. Li, J. Yan, and D. Tao, "St-p3: End-to-end vision-based autonomous driving via spatial-temporal feature learning," in *European Conference on Computer Vision*. Springer, 2022, pp. 533–549.

[65] P. Li, S. Ding, X. Chen, N. Hanselmann, M. Cordts, and J. Gall, "Powerbev: A powerful yet lightweight framework for instance prediction in bird's-eye view," *arXiv preprint arXiv:2306.10761*, 2023.

[66] Y. Hu, J. Yang, L. Chen, K. Li, C. Sima, X. Zhu, S. Chai, S. Du, T. Lin, W. Wang *et al.*, "Planning-oriented autonomous driving," in *Proceedings of the IEEE/CVF Conference on Computer Vision and Pattern Recognition*, 2023, pp. 17 853–17 862.

[67] T. Ye, W. Jing, C. Hu, S. Huang, L. Gao, F. Li, J. Wang, K. Guo, W. Xiao, W. Mao *et al.*, "Fusionad: Multi-modality fusion for prediction and planning tasks of autonomous driving," *arXiv preprint arXiv:2308.01006*, 2023.

[68] W. Luo, C. Park, A. Corrman, B. Sapp, and D. Anguelov, "Jfp: Joint future prediction with interactive multi-agent modeling for autonomous driving," in *Conference on Robot Learning*. PMLR, 2023, pp. 1457–1467.

[69] B. Wilson, W. Qi, T. Agarwal, J. Lambert, J. Singh, S. Khandelwal, B. Pan, R. Kumar, A. Hartnett, J. K. Pontes, D. Ramanan, P. Carr, and J. Hays, "Argoverse 2: Next generation datasets for self-driving perception and forecasting," in *Proceedings of the Neural Information Processing Systems Track on Datasets and Benchmarks (NeurIPS Datasets and Benchmarks 2021)*, 2021.

[70] S. Lee, T. Woo, and S. H. Lee, "Multi-attention-based soft partition network for vehicle re-identification," *Journal of Computational Design and Engineering*, vol. 10, no. 2, pp. 488–502, 02 2023.

[71] S. Lee, E. Park, H. Yi, and S. H. Lee, "StRDAN: Synthetic-to-real domain adaptation network for vehicle re-identification," in *Proceedings of the IEEE/CVF Conference on Computer Vision and Pattern Recognition (CVPR)*, 2020, pp. 608–609.

[72] S. Lee, T. Woo, and S. H. Lee, "SBNet: Segmentation-based network for natural language-based vehicle search," in *Proceedings of the IEEE/CVF Conference on Computer Vision and Pattern Recognition (CVPR)*, 2021, pp. 4054–4060.

[73] H. Eom and S. H. Lee, "Mode confusion of human-machine interfaces for automated vehicles," *Journal of Computational Design and Engineering*, vol. 9, no. 5, pp. 1995–2009, 2022.

[74] Y. Zhong and S. H. Lee, "Gazesymcat: A symmetric cross-attention transformer for robust gaze estimation under extreme head poses and gaze variations," *Journal of Computational Design and Engineering*, vol. 12, no. 3, pp. 115–129, 2025.

[75] R. Huang, H. Xue, M. Pagnucco, F. D. Salim, and Y. Song, "Vision-based multi-future trajectory prediction: A survey," *IEEE Transactions on Neural Networks and Learning Systems*, pp. 1–18, 2025.

[76] A. Rudenko, L. Palmieri, M. Herman, K. M. Kitani, D. M. Gavrila, and K. O. Arras, "Human motion trajectory prediction: A survey," *The International Journal of Robotics Research*, vol. 39, no. 8, pp. 895–935, 2020.



Minsang Kong is with the Department of Automobile and IT Convergence, Kookmin University, Seoul, South Korea. His research interests include autonomous driving technology, deep learning-based perception, trajectory prediction, and multi-agent behavior modeling. He is particularly interested in sensor fusion, object detection, and the application of artificial intelligence in real-world autonomous systems. He has received multiple awards for his research contributions and has actively participated in research projects on self-driving perception and prediction models. He has also contributed to the academic community through competitions and workshops.

Minsang Kong is with the Department of Automobile and IT Convergence, Kookmin University, Seoul, South Korea. His research interests include autonomous driving technology, deep learning-based perception, trajectory prediction, and multi-agent behavior modeling. He is particularly interested in sensor fusion, object detection, and the application of artificial intelligence in real-world autonomous systems. He has received multiple awards for his research contributions and has actively participated in research projects on self-driving perception and prediction models. He has also contributed to the academic community through competitions and workshops.



models. He has also contributed to the academic community through competitions and workshops.

Myeongjun Kim is with the Department of Automobile and IT Convergence, Kookmin University, Seoul, South Korea. His research interests include autonomous driving technology, deep learning-based perception, and multimodal trajectory prediction. He is particularly interested in sensor fusion, object detection, and end-to-end autonomous driving. He has received multiple awards for his research contributions and has actively participated in research projects on self-driving perception and prediction models. He has also contributed to the academic community through competitions and workshops.



Sang Gu Kang is with the Department of Automotive Engineering, Kookmin University, Seoul, South Korea. His research interests include artificial intelligence, autonomous driving, and deep learning-based computer vision, with a focus on object detection, V2X datasets, and trajectory prediction. He has contributed to sensor fusion and object detection for autonomous driving systems and participated in the DriveX Challenge at CVPR, where he received a third-place award.



Hejiu Lu received the B.S. degree in Automotive Engineering from Kookmin University, Seoul, South Korea, and is currently pursuing the Ph.D. degree at the Graduate School of Automobile and Mobility, Kookmin University. His research interests include artificial intelligence, autonomous driving, and deep learning-based computer vision, with a focus on object detection, trajectory prediction, and traffic accident analysis for autonomous driving.



settings for practical multimodal perception systems.

Yupeng Zhong received the B.S. and M.S. degrees in Automotive Engineering from Kookmin University, South Korea. His research focuses on multimodal computer vision and learning-based perception, with emphasis on multimodal fusion and representation learning for robust scene understanding. His interests include gaze estimation and autonomous driving perception. His current research further encompasses depth estimation and enhancing model robustness and generalization in real-world settings for practical multimodal perception systems.



Sang Hun Lee received the B.S., M.S., and Ph.D. degrees in Mechanical Design and Production Engineering from Seoul National University, Seoul, South Korea, in 1986, 1988, and 1993, respectively. From 1993 to 1995, he was a Senior Researcher with the Research Center of Sindo Ricoh Co. Since 1996, he has been a Professor with both the Department of Automotive Engineering and the Graduate School of Automobile and Mobility, Kookmin University.

Dr. Lee has authored more than 70 papers in international journals and conference proceedings. He currently serves as a Co-Editor-in-Chief of the *Journal of Computational Design and Engineering*. His research interests include intelligent vehicles, human-centered autonomous systems, human-machine interaction, computer-aided design, and the application of artificial intelligence in industry.